Build Simul (2023) 16: 2307–2331
https://doi.org/10.1007/s12273-023-1052-y

Double-skin façade simulation with computational fluid dynamics: A review of simulation trends, validation methods and research gaps

Simon Pommerencke Melgaard, Ivan Titov Nikolaisson, Chen Zhang, Hicham Johra, Olena Kalyanova Larsen (✉)

Department of the Built Environment, Aalborg University, Denmark, Thomas Manns Vej 23, 9220 Aalborg, Denmark

Abstract

Dynamic simulation of a double-skin façade (DSF) with computational fluid dynamics (CFD) can be challenging due to the lack of validated models and benchmarking datasets. Furthermore, there is a lack of consensus in the scientific community on what constitutes a successfully validated DSF model. The present review study identifies simulation trends and research gaps for DSFs simulated with CFD. Additionally, this article presents a series of CFD simulations in which key aspects of the DSF modelling are varied: 2D or 3D modelling approaches, turbulence viscosity models (TVMs), radiation models, and wall function. These simulation results are compared to the empirical data (both temperature and velocity fields) of a benchmark test with laboratory-controlled boundary conditions. This analysis shows that using the *k*-ε RNG model with enhanced wall treatment and surface-to-surface (S2S) radiation model yields the best results for the 2D case of natural convection flow. Moreover, it is shown that accounting for the velocity field in the validation process is essential to ensure the suitability of a model. Finally, the authors advocate for the use of selected dimensionless numbers to improve the comparability of the different DSF scientific studies. This would also help to identify relevant experimental datasets for validation and suitable CFD simulation settings for specific DSF cases.

Keywords

double-skin façade
ventilated cavity
computational fluid dynamics
empirical validation
modelling parameters
dimensionless numbers
convection

Article History

Received: 07 December 2022
Revised: 19 May 2023
Accepted: 03 June 2023

1 Introduction

The double-skin façade (DSF) concept dates back to the beginning of the 20th century or even further back (Saelens 2002; Barbosa and Ip 2014). It is thus well known to architects and engineers and has been alternately prized and criticised over the years. The enthusiasm about the concept is often explained by slick and large transparent surfaces, preservation of the aesthetics and visibility of underlying historical façades, possible integration of various dynamic envelope functionalities, potential energy performance improvement, reduction of outdoor noise level, and other valuable architectural features. The discussion of whether the concept should exist may continue, but it will certainly not disappear and, therefore, deserves some consideration. Over the past two decades, most of the DSF studies have focused on the following:

- Assessment and optimisation of DSF performances (Haddad and Elmahdy 1998; Manz et al. 2004; Takemasa et al. 2004; Ding et al. 2005; Gratia and De Herde 2007; Saelens et al. 2008; Seferis et al. 2011; Choi et al. 2019; Zhang and Yang 2019; Pourshab et al. 2020; Najaf Khosravi and Mahdavi 2021).
- Empirical validation of existing simulation tools (Kalyanova et al. 2009; Choi et al. 2012; Mateus et al. 2014; Catto Lucchino et al. 2021).
- Development of new numerical tools for accurate DSF modelling (Balocco 2002; von Grabe 2002; Faggembauu et al. 2003; Mei et al. 2003; Park et al. 2004; Dama et al. 2017; Inan and Basaran 2019; Tao et al. 2021a).
- Development of new performance metrics (Loonen et al. 2017; Soudian and Berardi 2021).
- Integration of adaptive technologies such as elastoplastic passive devices for mitigation of wind and earthquake effects (Amadio and Bedon 2012), spectrum-selective solutions (Favoino et al. 2014), bionic façade (Šuklje et al. 2013) and others.

The use of computational fluid dynamics (CFD) for

E-mail: ok@build.aau.dk

List of symbols

Nomenclature

CFD	computational fluid dynamics
DO	discrete ordinates
DSF	double-skin façade
DTRM	discrete transfer radiation model
LDV	laser Doppler velocimetry
PIV	particle image velocimetry
S2S	surface-to-surface
SA	Spalart-Allmaras
TVM	turbulence viscosity model

Dimensionless numbers

Ar	Archimedes number
$Aspr$	aspect ratio
Gr	Grasshof number
Pr	Prandtl number
Ra	Rayleigh number
Re	Reynolds number

Physical properties

C_p	specific heat capacity
D	depth
g	gravitational acceleration
H	height
k	thermal conductivity
L	length
T	temperature
u	velocity
β	expansion coefficient
ν	kinematic viscosity
ρ	density

Subscripts

amb	ambient
avg	average
char	characteristic
D	depth as the characteristic length
H	height as the characteristic length
surf	surface
surf_front_wall	surface of the front wall in the DSF case
surf_heated_backwall	surface of the back wall in the DSF case

performance evaluation and optimisation of DSF was not overlooked. In fact, the CFD approach seems to be the most comprehensive for studying the airflow and thermal exchange mechanisms at play in a DSF (Fuliotto et al. 2010; Pourshab et al. 2020; Lops et al. 2021). However, the complexity and intricacies of the dynamic airflow patterns and heat transfers in a DSF are far from being thoroughly understood (Fuliotto et al. 2010; Seferis et al. 2011; Dama et al. 2017; Inan and Basaran 2019; Najaf Khosravi and Mahdavi 2021). This might impair the proper design and optimisation of DSF systems, leading to building cases with poor performance and limiting the exploration of DSF's full potential.

Nowadays, CFD is routinely used in civil engineering when a large or complicated air distribution system has to be designed (Nielsen 2015). As argued by P. Nielsen in his review (Nielsen 2015), a CFD user must make some critical decisions before simulation, including selecting turbulence models, determining steady or transient simulation, generating 2D or 3D geometries, or defining reasonable boundary conditions. Many studies have been conducted to provide recommendations on selecting proper numerical schemes and models for indoor air movement. Chen (1995) compared different k-ε models for indoor airflow computations. Zhang et al. (2007) gave an overview of the characteristics of different turbulence models for various types of flow in ventilated space. Nielsen et al. (2007) developed a guidebook to support decision-making when using CFD in ventilation design. The development of CFD models for room air movement undoubtedly promotes the use of CFD for DSF heat and mass transfer prediction. However, the understanding of DSF performance using CFD tools is not yet at the same maturity level as the modelling of ventilated rooms. There is a lack of common agreement on which turbulence models and boundary conditions are suitable for DSF systems (Coussirat et al. 2008; Ahmadi et al. 2022). In addition, the lack of a benchmarking test is a challenge for the development of CFD for DSF. It is critical to test and adjust the CFD models by comparing simulated results against empirical benchmarking test datasets. The latter can support the selection of a turbulence model, the study of mesh independence, and the evaluation of numerical schemes and boundary conditions. Unfortunately, the currently available empirical data for DSF is often too coarse or with too high measurement uncertainty.

This article aims to extend the discussion on how to simulate DSF systems with CFD and shed some light on selecting key model parameters and settings. The article opens with a comprehensive literature study of the main DSF modelling aspects when using CFD, such as the

selection of turbulence viscosity models (TVMs), two- and three-dimensional modelling geometries, application of various boundary conditions, and validation procedures. In Section 3, we conducted a benchmarking test in a DSF setup with well-controlled steady-state boundary conditions. This was used to evaluate the accuracy of different CFD simulations with various TVMs and radiation models against empirical data. A grading system was also introduced to support the accuracy evaluation of different models. Finally, the article closes with general conclusions and suggestions for future work for DSF numerical modelling with CFD.

2 Key modelling aspects

Multiple decisions must be made when developing a high-quality CFD model of a DSF. The model results depend on the perspective from which the problem is analysed, the chosen modelling hypotheses, and the simulation settings (Lops et al. 2021). The current scientific literature typically addresses the following main aspects for modelling the airflow and thermal exchange mechanisms in a DSF: boundary conditions in the model, modelling of the radiation heat exchange, evaluation of the flow type for TVM selection, 2D or 3D geometries, presence of transient effects, and empirical validation. Accordingly, the current review study will touch upon all these key aspects.

2.1 Flow behaviour

Concerning CFD for room air movement, more than 50 years of research ensure a sufficient amount of well-documented and validated models and benchmark cases to select an appropriate TVM for specific flow types and geometries. However, few studies have been published for turbulent natural convection in vertical channels, such as in DSF (Ben-Mansour et al. 2007; Zhang and Yang 2019; Ahmadi et al. 2022). The same few experimental datasets were used to validate DSF CFD models until now. These are the experimental data acquired by Miyamoto et al. (1986), Manz et al. (2004), Mei et al. (2007), and Dama et al. (2017). Lately, new experimental data focusing on the flow structure and the velocity field evaluation has been released, such as Bhamjee et al. (2013) and Sánchez et al. (2019). The authors use the measurement techniques particle image velocimetry (PIV) or laser Doppler velocimetry (LDV), which allow better insight into the velocity field inside a DSF without disturbing the flow. Nevertheless, it does not change the fact that only a few studies about the flow structure and heat transfer in DSF exist. Even less is known about the potential transient characteristics of the flow in the DSF cavity (Zhang and Yang 2019). Gau et al. (1992) suggest that the flow inside a vertical heated channel has transient behaviour for $Ar > 48$. Therefore, comparing transient measurements and steady-state CFD models could be questionable since the mean value of the flow characteristics might not give a good representation of an intrinsically time-dependent system.

2.1.1 Flow type

Several factors define the flow regime; the first ones being the driving forces, which are either inertial or buoyancy forces. Inertial forces can be due to a mechanical component, such as a fan or strong wind forces. This type of flow is characterized by the Reynolds number, which indicates whether the flow is laminar, transitional, or turbulent. Buoyancy forces are primarily caused by temperature differences leading to variations in the density of the air inside the DSF, resulting in a buoyant flow. Buoyant forces are characterized by the Rayleigh number. The Archimedes number is used to distinguish whether the flow is inertial or buoyancy-driven (see Table 1).

Another essential factor to consider in non-isothermal conditions is the cavity aspect ratio height/depth, which is used to distinguish between narrow and wide cavities. The formula for defining the narrow or wide cavity can be seen in Eq. (2). In narrow cavities, the boundary layers merge and form a fully developed velocity profile. On the contrary, in wide cavities, the boundary layers do not interfere with each other. Thus, narrow and wide cavities have different characteristics regarding heat transfer. Following this logic, one can argue that the aspect ratio must be considered alongside the dimensionless numbers for selecting appropriate turbulence viscosity models.

2.1.2 Flow structure

Characterizing flow and heat transfer in naturally ventilated DSF cavities remains challenging. On the one hand, there is a lack of experimental data that can support the research community in forming meaningful hypotheses about the flow and heat transfer in the cavity to select an appropriate TVM. On the other hand, there is an absence of experimental data that describes the velocity profiles (including the boundary layer flow), characteristic flow features (such as local recirculation, counterflow, or zones with still air), steady/periodic/unsteady behaviour, and 3D effects. This greatly limits the process of model validation. Altogether, these elements describe the flow structure in the cavity and the resulting heat transfer. It is not clear yet if these elements should be included in the design of CFD models. In the study by Dama et al. (2017), different cases of naturally-induced flow are studied. The authors document the presence of either recirculation zones or reversed flow in the DSF. The occurrence of recirculation zones is also found experimentally in several articles with natural

convection in an asymmetrically heated vertical air channel, such as Habib et al. (2002) and Taieb et al. (2013). Popa et al. (2012) and Polidori et al. (2015) documented similar occurrences for water. Bhamjee et al. (2013) visualized the flow structure for naturally- and mechanically-ventilated supply air windows. They also reported recirculation/reversal of the flow along with the presence of steady and unsteady periods in the flow development. He and Lv (2022) documented similar effects for a solar chimney. Figure 1 and Figure 2 illustrate flow reversal and local recirculation flow elements (reproduced from Taieb et al. (2013) and Polidori et al. (2015)).

In 2013, Dupont et al. (2013) argued that the recirculation zones are related to the Rayleigh number and the aspect ratio. Recently, Cherif et al. (2020) published numerical and experimental work describing natural free convection in asymmetrically heated building structures, such as Trombe walls or ventilated windows. The authors draw an explicit link between the flow structure (including the characteristics of the DSF flow elements), the modified Rayleigh number, the aspect ratio, and the evolution of the thermal and velocity field. Thus, selecting an appropriate TVM can benefit from better insights to flow structure and evolution besides the knowledge of the flow regime. However, very few studies

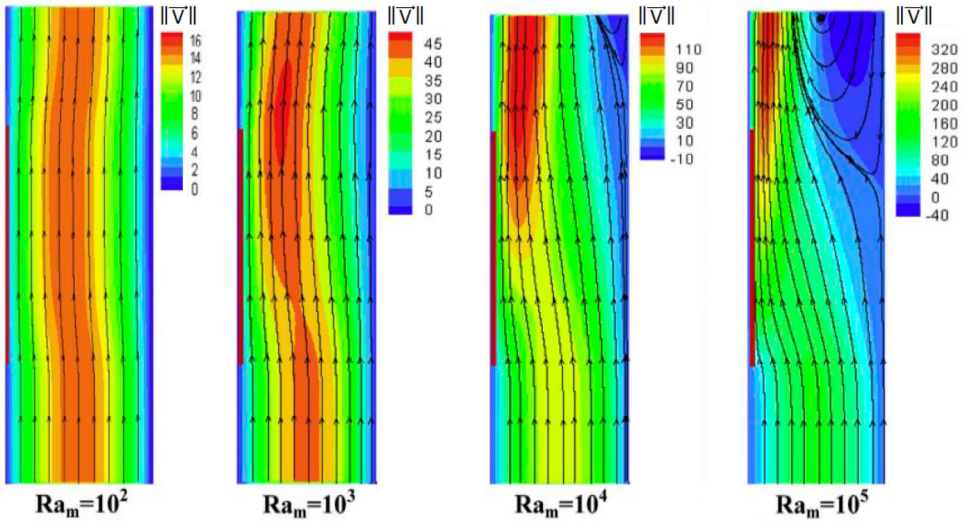

Fig. 1 Streamlines and vertical velocity field (dimensionless velocity components $\|\vec{V}\|$) for different modified Rayleigh numbers in the case of a simple channel. The figure is adapted from Taieb et al. (2013)

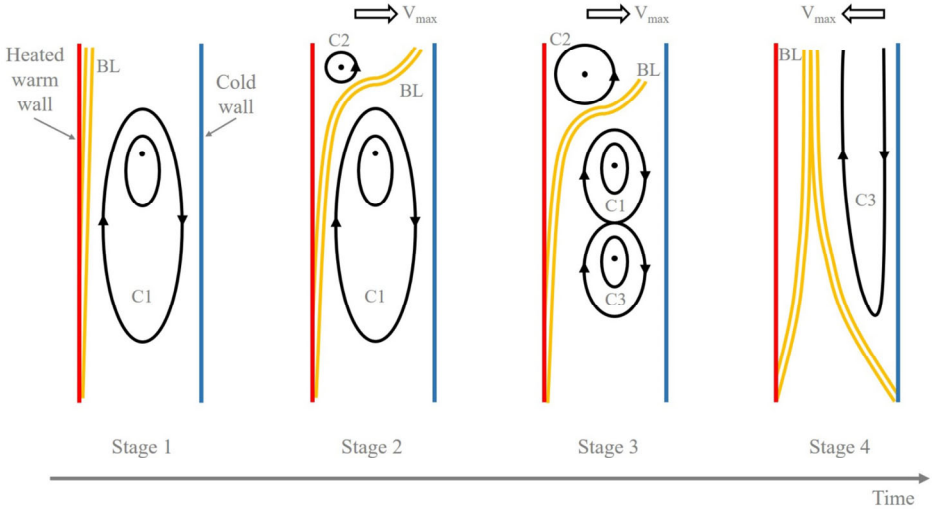

Fig. 2 Different development stages of the free convection flow with the establishment of a large-scale reversal flow in an asymmetrically heated open-ended channel: "C1", "C2", and "C3" correspond to recirculation cells; "BL" corresponds to the boundary layers; the arrow labelled "V_{max}" indicates the direction in which the horizontal velocities are increasing. Stage 1: the creation of a primary cell C1 due to fluid feeding of the hot boundary layer; Stage 2: boundary layer separation due to swelling of secondary cell C2; Stage 3: vortex splitting of the primary cell C1 into two co-rotating cells (C1 and C3); Stage 4: upward motion of C1, the disappearance of C2, junction of boundary layers and extension of C3 leading to a major reversal flow. The figure is adapted from Polidori et al. (2015)

systematically report the key dimensionless numbers of the DSF system, namely, the cavity aspect ratio and the Rayleigh number. This lack is an unfortunate shortcoming in the present scientific literature, which might partly explain the limited progress in CFD applications for different DSF typologies.

The cases shown in Figure 1 are steady-state situations. However, in the study by Polidori et al. (2015), it is found that recirculation in the asymmetrically heated channel is a time-dependent phenomenon that can be separated into four main steps (see Figure 2). A similar conclusion is made by Bhamjee et al. (2013). Thus, the question of modelling DSF can be related not only to turbulence model, boundary condition, and 2D/3D geometries but also to the transient behaviour.

2.1.3 Turbulence viscosity models

The choice of TVM is only discussed in a limited number of publications. Coussirat et al. (2008) tested the following TVMs: Spalart-Allmaras (SA), *k-ε* Standard, RNG, *k-ε* Realisable, *k-ω* Standard, and *k-ω* SST. The test was performed with the experimental data from Manz et al. (2004) for a metal shading screen in the middle of a mechanically-ventilated cavity, and according to the procedure described by Wilcox (1988) in which the measured air temperature at the exhaust opening is compared with the simulated one. It was found that the *k-ε* RNG model was the best-performing model. However, one should note that this study does not address the temperature field or the velocity field inside the DSF cavity. There is thus no guarantee that the internal airflow is the same as the reference monitored case.

A second study by Pasut and de Carli (2012) compared different TVMs for a naturally ventilated façade with a Venetian blind (see Figure 3(c) and Figure 3(d)). The *k-ε* RNG and *k-ω* SST models were evaluated under different boundary conditions and domains. The models are validated based on the experimental data from Mei et al. (2007), with temperatures and velocities measured at seven horizontally distributed points in the middle of the cavity. It was concluded that the *k-ε* RNG model predicts the temperature and velocity better than the *k-ω* SST model. Both the studies from Coussirat et al. (2008) and Pasut and de Carli (2012) document the better performance of the *k-ε* RNG model. However, it must be noted that both studies also include internal obstacles: either Venetian blinds or a metal shading screen.

Ben-Mansour et al. (2007) compared several turbulent models for predicting the natural convection flow and heat

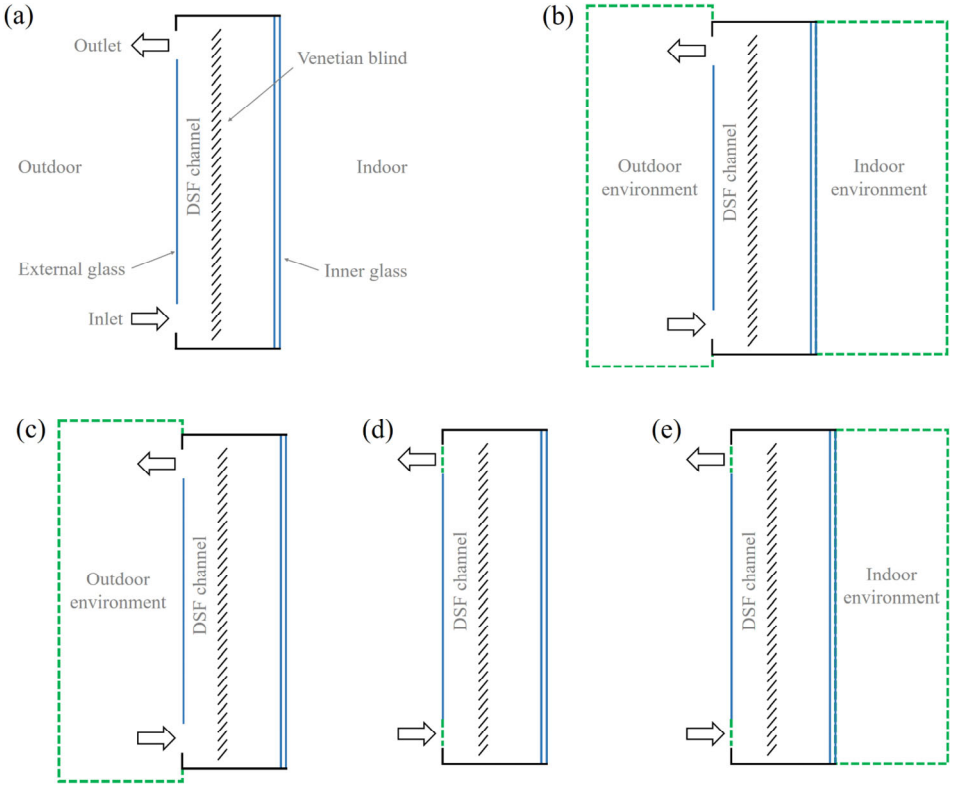

Fig. 3 Modelling strategies regarding the placement and implementation of boundary conditions (dashed green lines): (a) the schematic of the DSF case; (b) coupling the flow from the external and internal environments; (c) coupling the DSF flow with the external environment only; (d) decoupling the DSF flow with the internal and external environments; (e) coupling the DSF flow with the external environment only

transfer in vertical air channels. The authors conclude that the low Reynolds number k-ε model leads to more accurate results. The experimental data used for the validation is described by Miyamoto et al. (1986). Recently, Lops et al. (2021) analysed the implementation of the SST k-ω model, V2F and k-ε Realisable turbulence models against the experimental results of Dama et al. (2017). The authors conclude that all three models perform well compared to the empirical reference. All three models have similar velocity profiles but remain significantly different from the measurement data.

In work by Jiru et al. (2011), a mechanically ventilated DSF with a Venetian blind is simulated using the k-ε RNG. The authors stated that the k-ε RNG was more accurate and reliable than the k-ε Standard model for forced convection. However, they did not provide any references to support that statement. In the study by Fuliotto et al. (2010), the case was a DSF with Venetian blinds inside. The k-ε RNG model was employed because of its *"successful validation in the past"* (Chen 1995; Zhang et al. 2007). Zhang et al. (2007) state that the k-ε RNG model is generally suitable for indoor airflow. However, for flow in a tall cavity with a temperature gradient, it underpredicts the fluctuations of vertical velocity. The study by Brandl et al. (2014) used a 3D DSF without a Venetian blind and identified buoyancy as the main driving force. The authors selected the k-ε RNG model based on the findings from Coussirat et al. (2008). A review by Pourshab et al. (2020) underlines that the k-ε RNG model is preferable over other TVMs. However, the model is not extensively validated, as the experimental data used for validation is derived from Mei et al. (2007), which is characterised by a limited number of measurement points.

For studies not focusing on TVM comparison but applying full CFD models to real cases, the k-ε Realisable or the k-ε RNG models were generally selected. The k-ε Realizable was used by Safer et al. (2005) to model a single-floor DSF with a Venetian blind. The authors argue that this TVM is validated for channel and layer flow (Shih et al. 1995; Fluent 2006) and applicable to this configuration. It is also used by Hazem et al. (2015) to simulate a DSF with a Venetian blind. It is argued to be one of the most frequently used TVMs for laminar and transitional flow patterns. Presently, it remains uncertain to what degree the k-ε Realisable model is applicable for all cases, as both laminar and turbulent flow can occur in DSFs, depending on geometry and boundary conditions (Zhang and Yang 2019). However, to the best of the authors' knowledge, only a few publications acknowledge the significance of the flow regime for selecting the TVM, and none mention the importance of the flow structure.

From the literature study, it is also observed that most of the simulated cases have Venetian blinds. Therefore, it is uncertain whether the TVMs presented in those studies also apply to cases without Venetian blinds. The flow structure in cases with and without the blinds can differ due to the potential flow obstruction or additional heat source in the cavity. Studies that model the DSF with Venetian blinds tend to use k-ε Realisable or k-ε RNG. The choice of TVM for modelling a DSF without Venetian blinds appears less consistent. Dama et al. (2017) use the k-ω SST and justify this choice with a study by Bangalee et al. (2013). Angeli and Dama (2015) use the q-ζ and k-ε Lauder-Sharma to handle the incompressible and compressible flow, respectively. Brandl et al. (2014) employ the k-ε RNG model, stating that "*recent literature research showed a large number of papers using this TVM for CFD simulations of ventilated façades and double pane windows*". To conclude on that matter, a more extensive study is needed, as there seems to be a lack of consensus as to which TVM should be used for DSF without Venetian blinds.

2.2 Boundary conditions

Iyi et al. (2014) recommended modelling the DSF separately, as in Figure 3(d), unless the outdoor or indoor boundaries are essential for airflow or heat transfer. It is explained that the external or internal environment does not seem to introduce a significant change in the thermal behaviour of the DSF cavity. A different conclusion was, however, drawn in a study by Pasut and de Carli (2012). The former tested the effect of the presence of the exterior environment in the model (see Figure 3(c) and Figure 3(d)). The study concludes that "*the external environment modelisation is important for the simulation quality. An adequate ambient air frees the user from deciding the air inlet direction and makes this more reliable*." Thus the question remains on whether or not the external domain can be neglected in favour of well-defined thermal and velocity boundaries. Consequently, what does constitute well-defined thermal boundary conditions? Other scientific works based on Mei et al. (2007) were published later using the same model settings (Kim 2021) or experimental dataset (Pourshab et al. 2020; Tao et al. 2021b) for validation. Tao et al. (2021b) investigated the effect of the glazing characteristics on the performance of buoyancy-driven ventilation in a DSF. They defined the geometric domain as in Figure 3(b) and used the discrete ordinates (DO) model to solve the radiation for the semi-transparent surfaces.

Looking at the dynamic boundaries for the inlet and outlet openings, Safer et al. (2005) investigated the modelling of DSF by defining the velocity boundary for the inlet as fixed velocity and configuring the turbulence intensity. The outlet was defined as an outflow boundary, assuming a fully developed flow. Coussirat et al. (2008) modelled the

mechanically-driven flow as velocity boundaries with a constant outflow. Jiru et al. (2011) conducted a study where the simulated boundary conditions were defined according to the schematics in Figure 4 for the mechanically driven flow. The outflow was set with a constant volumetric flow rate and temperature.

He and Lv (2022) modelled a solar chimney, where the inlet and outlet were treated as zero-pressure openings with resistance coefficients to address the potential flow reversal at the outlet (top opening). The same approach is used by Lops et al. (2021) for naturally ventilated cavities where the thermal boundaries are defined as a constant temperature field (extracted from measurement data produced by Dama et al. (2017)) and imposed on all surfaces of the DSF. The wind effect on the naturally ventilated cavity was studied by Matour et al. (2021). An atmospheric wind profile was imposed at the inlet boundary. The outlet boundary condition was set to outflow, while the ground and building's surfaces were set to no-slip wall.

One of the challenges in modelling the thermal boundary for DSF is to include the impact of radiation on the façade. For example, should the radiation be simulated directly (Coussirat et al. 2008; Jiru et al. 2011; Brandl et al. 2014; Iyi et al. 2014; Hazem et al. 2015), as a heat flux (Gan 2006; Coussirat et al. 2008; Iyi et al. 2014; Hazem et al. 2015), or as a constant temperature boundary (Fuliotto et al. 2010; Pasut and De Carli 2012; Dama et al. 2017; Kim 2021)? This depends on the available information and how simple a model ought to be. Changing the boundary conditions from radiation modelling to either a constant temperature or a heat flux field adds limitations to the generalisation potential of the model. Indeed, it would require the measurement of surface temperatures or heat flux and can potentially eliminate the 3D effects originating from solar radiation. In Dama et al. (2017) and Lops et al. (2021), the same experimental data is used to define the uniform temperature conditions imposed on all surfaces. The same approach is used in Kim (2021) and Pasut and De Carli (2012) with another dataset. Recently, a numerical and experimental study of natural convection in DSF was conducted by Cherif et al. (2020), who studied two cases independently: one with a constant heat flux and one with a constant temperature boundary. The DSF was modelled with one wall being maintained at the heating condition and the other insulated. For the case with the constant temperature, the radiative heat transfer was not included in the model.

In Brandl et al. (2014), the thermal boundary conditions for the inner and outer layers are defined as walls with integrated virtual layers exposed, corresponding to internal and external temperatures. In order to account for the thermal effect of the incoming solar radiation, heat sources

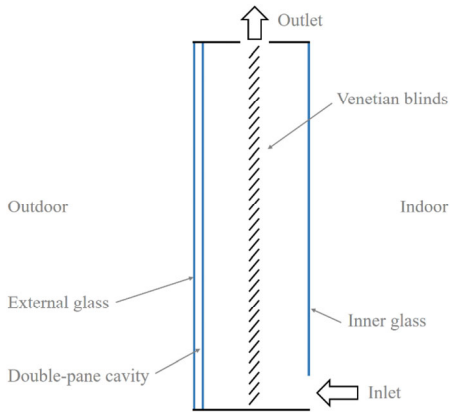

Fig. 4 Mechanically ventilated DSF configuration in the numerical study of Jiru et al. (2011). The figure is adapted from Jiru et al. (2011)

were added to the wall surfaces using the measured solar radiation with consideration of the material optical properties. In the studies by Iyi et al. (2014) and Coussirat et al. (2008) (see Figure 3(d)), the exterior layer was treated as a convective and radiative flux, and the interior layer was a convective heat flux. A constant value of 12 W/(m^2·K) for the heat transfer coefficient was derived from experimental measurements on the exterior layer. The radiation boundary was computed with a radiation model. A value of 8 W/(m^2·K) was used for the convective heat transfer coefficient of the indoor layer. Additionally, the solid surfaces are modelled with the no-slip boundary conditions. In the study by Hazem et al. (2015), the inner surfaces of the cavity and the slat surfaces were treated with coupled wall conditions. A mixed condition of radiation and convection was applied to the outer surfaces (exterior and interior glazing). The glazing elements were modelled as semi-transparent solids, and the blinds as opaque solids.

What generally appears to be the trend in the literature is that the surfaces are either modelled as a constant temperature field, thus neglecting the radiation model, or with heat fluxes. In such cases, the solar radiation is either converted into part of the heat flux or handled by a radiation model.

2.3 Radiation models

The decision about the treatment of radiation in CFD is closely related to the definition of the thermal boundary conditions and remains a delicate issue for open cavities (Desrayaud et al. 2013), both for shortwave (solar) and longwave radiation. Coussirat et al. (2008) studied the question. Three different radiation models were investigated for the case of a mechanically ventilated DSF with a metal shading screen. These models were the discrete transfer radiation model (DTRM), the DO model, and the P-1

radiation model. The radiation was included as a heat flux on the external boundary. One can see in Figure 5 that the P-1 model seems to predict best the temperature of the solids in the DSF. However valuable, this study has a limitation, as all conclusions are derived from a single measurement point in the cavity, which does not necessarily represent the behaviour of the whole DSF. A recent study published by Ahmadi et al. (2022) compared the airflow and the heat transfer in a naturally ventilated DSF for two types of thermal boundary conditions: (1) using constant temperature on the DSF surfaces; (2) modelling solar radiation by the DO model. Simulation results were obtained for a case study by Mei et al. (2007) and compared against their published experimental data. They document nearly the same results for both cases but argue for the application of the radiation model if the flow structure in the cavity is of interest.

The DO model is also used for a DSF with an integrated Venetian blind in Hazem et al. (2015). The model is validated experimentally, and the authors argue that this model can calculate the radiation at semi-transparent constructions (glass) and can handle non-grey radiation. Brandl et al. (2014) and Pastori et al. (2021) use the DO model to account for the long-wave radiation. In the case of a DSF with natural convection and a Venetian blind, Iyi et al. (2014) have chosen the DO model. Sánchez et al. (2019) used the DO model to account precisely for the effect of direct, diffuse, and ground-reflected solar radiation on the surface of an open joint ventilated façade. The DO model was also used by Tao et al. (2021b). They argue that the DO model is the only functional model for solving radiation with semi-transparent media. In this particular study, the researchers focused on the ventilation performance of naturally ventilated DSF with Low-E glazing, thus justifying the use of the DO model. An alternative approach to radiation

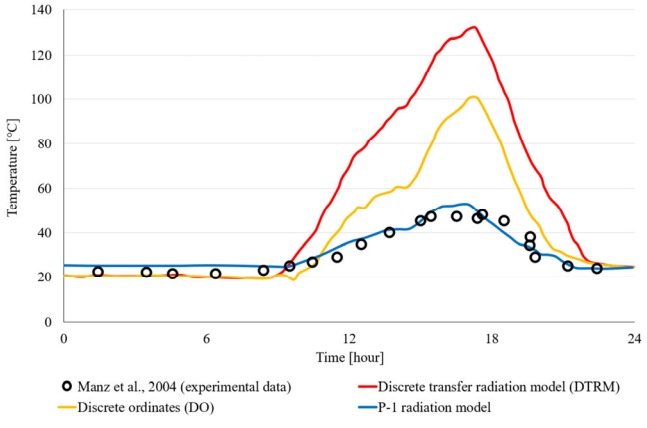

Fig. 5 Performance of different radiation models in the CFD study of Coussirat et al. (2008) compared to experimental results from Manz et al. (2004). The figure is adapted from Coussirat et al. (2008)

in a CFD model can be to use a different fluid, for example, water, in which radiation can be neglected. This has been done by Popa et al. (2012). This method is, however, only applicable if the convection term is significantly larger than the radiation term, as described in Guardo et al. (2011).

Recently, Choi et al. (2019) studied the cooling energy performance of a naturally ventilated DSF with a surface-to-surface model (S2S), similar to earlier studies by Jiru et al. (2011). However, the reasoning behind the choice of the radiation model by Jiru et al. (2011) is not specified, and the temperature discrepancies between the experiment and the model appear to be up to 5 °C. Lastly, the model performance in terms of the velocity distribution compared to the experimental data is absent and, therefore, does not allow for a fair evaluation of the results.

Another approach is to remove the radiation model and include the radiation as a heat flux or a constant temperature field and consider the glass boundary an opaque solid. This approach was adopted by the literature (Gan 2006; Fuliotto et al. 2010; Pasut and De Carli 2012; Angeli and Dama 2015; Dama et al. 2017; Pastori et al. 2021; Ahmadi et al. 2022). Generally, a more extensive study is needed to investigate different methods to model radiation in DSF and to advise about the pros and cons of using those. The paper from Coussirat et al. (2008) concludes that DO and DTRM can overpredict the temperature in the middle of the metalised shading screen by up to 80 °C. Contrary to Coussirat et al. (2008), several other studies find the DO model more accurate. Iyi et al. (2014) state that "*… to simulate the heat transfer due to radiation, Discrete Ordinate Method has been chosen due to its proven superiority in predicting radiative heat transfer involving a participating medium...*" referring to Chandrasekhar (1960), Hottel and Sarofim (1967) and Modest (1993). A similar statement is made by Tao et al. (2021b): "*…In ANSYS Fluent software, the DO model is the only functional model in solving radiation with semi-transparent media.*"

2.4 2D and 3D models

Different approaches have been adopted to model DSF geometries with different numbers of dimensions. Some studies model the DSF in 2D, which is considerably lighter computationally than 3D. The trade-off being 2D simulations cannot depict naturally occurring effects that 3D fluid flow might have. Several studies support that the 2D model is sufficient to simulate the airflow pattern in the ventilated cavity because the flow is close to two-directional. Fuliotto et al. (2010) conducted a study with Venetian blinds and compared the results of 2D and 3D models. It concluded that the temperature distribution was close to being two-dimensional in all sections apart from areas near the

inlet (where recirculation happens inside the DSF) and the outlet. The study concludes that two-dimensional simulations are acceptable for the given flow structure. A similar study was carried out by Pasut and de Carli (2012). They concluded that no remarkable changes in the temperature and velocity fields were observed when switching from a 2D to a 3D model. The same finding was also presented by Gan (2006) and Lops et al. (2021), pointing towards the adequacy of 2D simulations for DSFs.

However, there are several scenarios where 2D modelling might not be sufficient. This is the case for asymmetrical geometry. Safer et al. (2005) conducted simulations for a ventilated cavity with Venetian blinds. For the symmetrical case, a 2D model with a mesh size of 500 000 elements could provide sufficient accuracy. On the other hand, in the asymmetrical case, the authors argue for the use of a 3D model. The asymmetry can also be caused by wind driving forces, where the wind pressure may require spatial definition and cannot be adequately represented in 2D models. For example, Matour et al. (2021) investigated wind-driven ventilation in DSF. A 3D model was employed to address the wind effect. The presence of 3D effects on the flow structure in the DSF with vertical openings was clear. For simplicity reasons, most published models do not consider the wind effects for the naturally-driven flow in DSF (Pourshab et al. 2020), thereby reducing potential 3D effects in the models.

In addition, when a radiation model is used for the definition of the thermal boundary condition, it is expected that a 3D model is used to calculate the view factors between the different surfaces of the DSF and distribute the solar or surface radiation properly (Manz et al. 2004; Guardo et al. 2011; Radhi et al. 2013; Tao et al. 2021b). Several of these studies address solar beam radiation with different solar incidence angles and natural convection, indicating the presence of 3D effects. A symmetrical geometry with particularly pronounced 3D effects (spatial variation of the glazing surface temperature under the different solar incidence angles) is presented by Radhi et al. (2013).

2.5 Summary and discussions of previous studies

Table 2 gives an overview of the key articles about DSF flow and a few about asymmetrically heated channel flow. The DSF flow is typically understood as the flow in a ventilated DSF cavity. If the cavity is narrow, it can be classified as a channel flow. The definition of wide and narrow cavities is provided hereafter in the article.

Table 2 includes the key modelling aspects considered in the publications, along with the dimensionless numbers characterising those specific cases. In several publications, dimensionless numbers are not provided. The latter have thus been calculated according to the definitions in Table 1 and the information found in the corresponding publications, assuming that the reference point is in the middle of the cavity.

The dimensionless numbers in Table 1 are written in scientific notation according to Eq. (1) below:

$$N = a \cdot 10^{b} \quad \text{if} \quad 0.5 < a \leq 5 \tag{1}$$

where N is the dimensionless number [—]; a is the significant digits [—]; b is the power [—]; 10^b is the order of magnitude [—].

From the data of the studies presented in Table 2, it was possible to calculate an estimate of the Ra_H and the aspect ratio for each specific case. Figure 7 thus provides an easy way to identify what thermofluidic phenomena have been investigated in the literature until now. Figure 7 is available in an interactive format, with the possibility of filtering the data (Melgaard et al. 2023). The figure is developed using

Table 1 Various dimensionless numbers

Dimensionless number	Equation	Description
Reynolds number (Re)	$Re = \frac{u L_{char}}{\nu}$	Ratio of the inertial forces to the viscous forces (Incropera et al. 2007)
Grashof number (Gr)	$Gr = \frac{g \beta (T_{surf} - T_{amb}) L_{char}^3}{\nu^2}$	Ratio of the buoyancy forces to the viscous forces (Incropera et al. 2007)
Prandtl number (Pr)	$Pr = \frac{\nu}{\alpha}; \alpha = \frac{k}{\rho c_p}$	Ratio of the momentum and thermal diffusivities (Incropera et al. 2007)
Rayleigh number (Ra)	$Ra = Gr \cdot Pr = \frac{g\beta (T_{surf} - T_{amb}) L_{char}^3}{\nu\alpha}$	Ratio describing when the heat transfer of the flow transitions between conduction and convection (Allaby 2008)
Archimedes number (Ar)	$Ar = \frac{Gr}{Re^2} = \frac{g\beta (T_{surf} - T_{amb}) L_{char}}{u^2}$	Ratio of the gravitational forces to the viscous forces (Li 2007)
Aspect ratio ($Aspr$)	$Aspr = \frac{H}{D}$	The ratio between the height and depth of the cavity

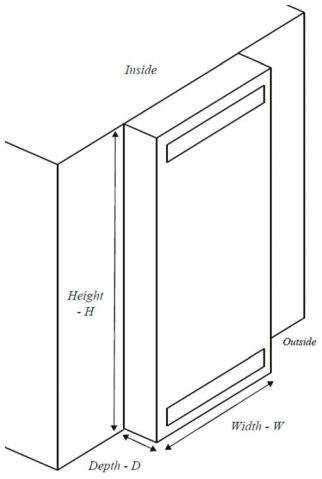

Fig. 6 Height, depth and width definition of the DSF

convective heat transfer theory (Bejan 2013) to describe the limit between the narrow and wide cavities. This limit between wide and narrow cavities is based on the inverse aspect ratio and the Rayleigh number (considering the channel's height or depth (see Eq. (2) (Saelens 2002)).

$$\frac{D}{H} > Ra_H^{-\frac{1}{4}} \quad \text{or} \quad \frac{D}{H} > Ra_D^{-1} \tag{2}$$

where H is the height [m]; D is the depth [m]; Ra is the Rayleigh number [—]. The definition of DSF height and depth can be seen in Figure 6.

Figure 7 shows that the reviewed scientific publications primarily study the wide cavities. Furthermore, it allows identifying studies with similar boundary conditions and, therefore, the similar flow structure, which can help for the in-depth evaluation of TVM and radiation models.

2.5.1 *Turbulence viscosity models*

It is generally assumed that the *k-ε* RNG model is the most

Table 2 Overview of previous studies on DSF using CFD. This data can be visualised in an online interactive table by Melgaard et al. (2023)

Study	Flow type and characteristics	Domain and geometry	Boundary conditions/driving force(s)	Radiation model(s)	TVM(s)	Experiment or validation/references	Conclusion	Comments	Dimensionless numbers (range and order of magnitude)
DSF flow									
Angeli and Dama 2015	• Turbulent flow. • Steady state. • Wide cavity. • Mixed convection. • Buoyancy- and wind-driven flow.	• Modelled in 2D. • Single floor DSF based on the measurements by reference (A).	• All glazed surfaces of the façade and the ground and ceiling have been imposed with constant uniform temperatures. • Outdoor air temperature of 19.2 °C.	• Not implemented (replaced with constant temperatures).	• *q-ζ*. • Lauder-Sharma low *Re k-ε*. • They were used because of the available TVMs in OpenFOAM®.	• No experiment. • Validation based on reference (A). •References: (A) Kalyanova and Heiselberg (2008).	• Both TVMs have problems predicting the full behaviour of the DSF. – L-S *k-ε* underestimates the temperature difference and the heat flux. – *q-ζ*- underestimates the mass flow rate and thereby also the heat flux.	• A simplified model for predicting the temperature difference, mass flow rate and heat flux was tested against the CFD model and proved more accurate but extremely sensitive towards the discharge coefficient. • Performed with significant assumptions.	• $Aspr$=9 • Pr=0.73 • Gr_D=10^8 • Ra_D=10^8 • Re_D=10^3 • Ar_D=10^1
Brandl et al. 2014	• Turbulent flow. • Unsteady state. • Wide cavity. • Mixed convection. • Buoyancy-driven flow.	• Modelled in 3D. • Panel-based DSF. • Located in Stallhofen, Austria.	• Pressure inlet, based on the external temperature of the inflow air. • Pressure outlet, based on the external temperature of the inflow air. • Symmetry at the left and right boundaries. • Interior glass surface has a temperature between 38 and 44°C. • External air temperature of 30°C. • Solar radiation converted to a boundary heat source.	• DO.	• *k-ε* RNG is used because it is suitable for a turbulent flow, reference (A).	• Performed experiment. • Validation based on own data. • References: (A) Coussirat et al. (2008).	• Applying side openings to the DSF increases the ventilation rate.	• The points used for validation are also used as boundary conditions.	• $Aspr$=22 • Pr=0.72 • Gr_D=10^6 • Ra_D=10^6 • Re_D=10^3 • Ar_D=10^{-2}–10^0
Coussirat et al. 2008	• Turbulent in the inner gap. • Potentially laminar in the outer gap. • Steady state. • Mixed convection.	• Modelled in 3D, but only with a width of 10 mm: – In order to be able to perform suitable modelling of the turbulence. – To use solar load radiation models that are only available in 3D.	• The outlet was a mass flow outlet, with a constant value of 0.1310kg·m^{-2}·s^{-1}). • The exterior façade was imposed with convective and radiative heat flux. • The internal façade was made with convective heat flux.	• DTRM. • DO. • P-1.	• Spalart-Allmaras. • *k-ε* Standard. • *k-ε* RNG. • *k-ε* Realisable. • *k-ω* Standard. • *k-ω* SST.	• No experiment. • Validation based on reference (A). • References: (A) Manz et al. (2004).	• The best-performing TVM was the *k-ε* RNG. • The best-performing radiation model was the P-1 model. • Gravitational forces are important to model buoyancy-affected flow. • CFD can be used to model the convection, conduction and heat transfer in a DSF.	• The grid independence test appears only tobe based on the exhaust temperature.	• $Aspr$=12 • Pr=10^{-1} • Re_D=10^2–10^3
Dama et al. 2017	• Turbulent flow. • Unsteady state. • Wide cavity. • Mixed and natural convection. • Buoyancy and wind-driven flow.	• Modelled in 2D. • Single floor DSF based on the measurements by reference (A).	• All glazed surfaces of the façade and the ground and ceiling have been imposed with constant uniform temperatures.	• Not implemented (replaced with constant temperatures).	• *k-ω* SST.	• No experiment. • Validation based on reference (A). • References: (A) Kalyanova and Heiselberg (2008).	• U-RANS CFD with well-posed boundary conditions can provide insight into the flow phenomena occurring in a DSF.	• Experienced reverse flow in the DSF.	• $Aspr$=9 • Pr=0.73 • Gr_D=10^8 • Ra_D=10^8 • Re_D=10^3–10^4 • Ar_D=10^0–10^2

Table 2 Overview of previous studies on DSF using CFD. This data can be visualised in an online interactive table by Melgaard et al. (2023) (Continued)

Study	Flow type and characteristics	Domain and geometry	Boundary conditions/driving force(s)	Radiation model(s)	TVM(s)	Experiment or validation/references	Conclusion	Comments	Dimensionless numbers (range and order of magnitude)
Fuliotto et al. 2010	• Turbulent flow. • Steady state. • Wide cavity. • Mixed and natural convection.	• Modelled in both 2D and 3D. • Venetian blinds. • Single-floor DSF test room. • Located at San Vendemiano, Italy.	• Inlet modelled as a pressure inlet with zero gauge pressure and a turbulence intensity of 15%. • Mechanically controlled exhaust fan, with a flow rate of 40m^3/h. • Four different cases with varying constants: – External temperature (28–32°C). – Room temperature (24–27°C). – Inlet air temperature (33–40°C). – Incident radiation (556–720 W/m^2).	• Not used. • Taken into account using the Boundary conditions.	• *k-ε* RNG is used because it is recommended in references (A) and (B).	• Did experiment. • Validation based on own data. • References: (A) Zhang et al. (2007), (B) Chen (1995).	• The velocity field is three-dimensional. • The thermal field behaves two-dimensionally.	• Reference (A) says the TVM can be used for DSF but that it is not good at predicting velocity fluctuations. • Reference (B) is only used for indoor airflow, not DSF.	• $Aspr$=31 • Pr=0.72 • Gr_D=10^6 • Ra_D=10^6 • Re_D=10^2 • Ar_D=10^0–10^1
Gan 2006	• Turbulent flow. • Steady state. • Wide cavity. • Natural convection. • Three different inlet positions.	• Modelled in 2D (assumed that cavity width was significantly larger than cavity depth). • With an inlet from outdoor, there are 1 inlet and 1 outlet. • With an inlet from indoor, there are 4 inlets (20 cm high) and 1 outlet. • With the inlet from indoor, there are 4 inlets (varied by floor, total area is the same as outlet) and 1 outlet.	• Heat flux on both sides of the cavity.	• Not used (because solar radiation was calculated before simulation and made into a heat-flux).	• *k-ε* Standard. • *k-ε* RNG.	• No experiment. • Validation based on reference (A). • References: (A) Sandberg and Moshfegh (1996).	• Used *k-ε* Standard because it was just as accurate as *k-ε* RNG, but with a coarser grid.	• The choice of TVM was made using a PV wall with only 1 inlet. • The DSF with 4 inlets might behave differently (rotations and turbulence).	• $Aspr$=12– 30 • Pr=0.73 • Gr_D=10^{11}– 10^{12} • Ra_D=10^{10}– 10^{12} • Re_D=10^4–10^4 • Ar_D=10^2–10^3
Hazem et al. 2015	• Both laminar and turbulent flow. • Steady state. • Wide cavity.	• Modelled in 2D. • Venetian blinds. • Single floor DSF.	• The inlet has a constant velocity, which is varied between 0.1 and 0.35 m/s. • The inlet has a constant temperature of 29 °C. • The inlet has a turbulence intensity of 6%. • The outlet is modelled as an outflow with a factor of 1. • Internal and external glazed surfaces have a radiative and convective heat flux. • Solar radiation is obtained on the external glass using the Bird model in two spectral bands (reference (B)).	• DO, used because it allows the simulation of non-gray radiation	• *k-ε* Realisable is used because: – It is one of the most frequently used models. – Can handle both laminar and transitional flow patterns at the same time.	• No experiment. • No validation. • References: (A) Safer et al. (2005), (B) Bird and Riordan (1986), (C) Safer (2006)	• The position of the blind angle is very influential in regards to the amount of heat gained through the DSF.	• Simulations are based on the geometry of the test cell (case (a)) in reference (A) • Lacks validation, even though the CFD model matches the CFD from reference (C), but none of the CFD models are backed up by experimental data.	• $Aspr$=15 • Pr=0.72 • Gr_D=10^7 • Ra_D=10^7 • Re_D=10^3 • Ar_D=10^0– 10^1
Iyi et al. 2014	• Turbulent flow. • Steady state. • Wide cavity. • Buoyancy-driven flow.	• Modelled in 3D. • Venetian blinds. • Single floor DSF based on the experimental data from reference (A). • Domain can be with or without: – External domain. – Internal domain.	• The air ingress and egress are modelled with zero gauge pressure. • Glass is modelled as semitransparent solids with a two-band spectral model (above or below 2.7μm). • Venetian blinds are modelled as opaque solids. • The external glass has a convective/radiative heat flux. • The internal glass has a convective heat flux. • The top and bottom walls are adiabatic. • If the internal/external domain(s) are modelled, then they have a constant temperature of 20°C.	• DO method has been chosen due to its proven superiority in predicting radiative heat transfer involving a participating medium; see references (B), (C), (D).	• Launder-Sharma low-*k-ε* is justified when the *y+* is below 1.	• No experiment. • Validation based on reference (A). • References: (A) Mei et al. (2007), (B) Chandrasekhar (1960), (C) Hottel and Sarofim (1967), (D) Modest (1993).	• The information on solar and thermal characteristics is crucial for realistic simulations. • If the boundary conditions are sufficiently specified, the thermal field is the same, whether or not the surrounding domain is modelled.	• Does not show a comparison with velocity between the experiment and numerical study. • Temperature comparison between the experiment and numerical study appears to show a potentially large difference even though the trend appears similar.	• $Aspr$=3.5 • Pr=0.73 • Gr_D=10^8 • Ra_D=10^8
Jiru et al. 2011	• Turbulent flow. • Steady state. • Wide cavity. • Mixed and natural convection. • Mechanically driven flow.	• Modelled in 2D. • Made both with and without Venetian blinds. • Based on an earlier experiment on a test cell located in Torino, Italy (reference (A)).	• Inlet was modelled with zero gauge pressure and a constant temperature of 20°C. • Outlet was an outflow with a constant flow rate of 54 m^3/h and an exhaust temperature of 25°C. • Internal wall was made with a constant heat flux of 8 W/(m^2·K). • External wall was made with a constant heat flux of 29 W/(m^2·K). • Outside temperature of 17°C.	• S2S is used without a specific reason.	• *k-ε* RNG is used because it is said to be more accurate and reliable for a wider class of flows than the standard *k-ε* model, though there is no source to back up the statement.	• No experiment. • Validation based on reference (A). • References: (A) Jiru and Haghighat (2008).	• Venetian blinds have an influence on the behavior of the DSF.	• Validation data remarks: – Discrepancies between measured and calculated temperatures of up to 4°C. – Cavity temperature is overestimated. – Blind temperature is underestimated. – No data for air velocity. • Simulation performed with measured max values and average flow rate.	• $Aspr$=17 • Pr=0.73 • With blinds – Gr_D=10^6 -10^7 – Ra_D=10^6 – Re_D=10^3 – Ar_D=10^0–10^1 • Without blinds – Gr_D=10^5 – Ra_D=10^5 – Re_D=10^3 – Ar_D=10^{-1}

Table 2 Overview of previous studies on DSF using CFD. This data can be visualised in an online interactive table by Melgaard et al. (2023) (Continued)

Study	Flow type and characteristics	Domain and geometry	Boundary conditions/driving force(s)	Radiation model(s)	TVM(s)	Experiment or validation/references	Conclusion	Comments	Dimensionless numbers (range and order of magnitude)
Pasut and de Carli 2012	• Turbulent flow. • Steady state. • Wide cavity. • Mixed and natural convection. • Buoyancy-driven flow.	• Modelled in 2D and 3D. • Venetian blinds. • Single floor DSF, based on the experimental data from reference (A).	• The air ingress/egress are modelled with zero gauge pressure. • The solar radiation was implemented as a constant temperature on the outside surface. • The indoor and outdoor temperatures are 20°C. • The simulations are run both with and without the external environment.	• Not implemented (because the radiation is a constant temperature boundary condition).	• k-ε RNG. • k-ω SST. • Used because they are two of the most popular TVMs.	• No experiment. • Validation based on reference (A). • References: (A) Mei et al. (2007).	• Using an adequate amount of ambient air makes the inlet air direction more reliable. • If the flow is bidirectional (or close), 2D simulations are preferred as they give the same results as 3D but are faster to run. • The k-ε RNG model performs best. • The operating density has an influence on how the velocity field behaves.		• $Aspr$=3.5 • Pr=0.73 • Gr_D=10^8 • Ra_D=10^8 • Re_D=10^3–10^4 • Ar_D=10^0–10^2
Safer et al. 2005	• Turbulent flow. • Steady state. • Mechanically controlled flow.	• Modelled in both 2D and 3D. • Venetian blinds modelled realistically in 2D. • Venetian blinds modelled as a porous media in 3D.	• Inlet modelled as a velocity inlet. • Inlet velocity of 0.10m/s. • Inlet turbulence intensity of 6%. • Outlet velocity modelled as an outflow.	• Not taken into account.	k-ε Realizable is used because it is validated for channel and layer flow (reference (A) and (B)).	• No experiment. • No validation. • References: (A) Fluent (2006), (B) Shih et al. (1995).	• A Venetian blind can be replaced by a porous media in 3D to decrease the grid size.	• Not validated with any experiments. • Energy equation neglected, as forced convection is assumed.	• $Aspr$=15 • Re_D=10^1–10^3
Xamán et al. 2005	• Laminar, transitional and turbulent flow. • Steady state. • Wide cavity. • Closed cavity.	• Modelled in 2D.	• The model consisted of walls with constant temperature: – The warm wall was kept at 25°C. – The cold wall was kept at 15°C. • The temperature gradient at the top and bottom walls is zero (adiabatic).	• Not used.	• k-ε models: – JL (reference(A)) – CH (reference(B)) – IL (reference(C)) – HH (reference(D))	• No experiment • Validation based on reference (E) • References: (A) Jones and Launder (1972), (B) Chien (1982), (C) Ince and Launder (1989), (D) Henkes (1990), (E) Dafa'Alla and Betts (1996).	• The Nusselt number increases if the aspect ratio increases for the turbulent case. • The Nusselt number decreases if the aspect ratio increases for the laminar case.		• $Aspr$=20–80 • Ra_D=10^2–10^8
Channel flow									
Habib et al. 2002	• Turbulent flow. • Steady state. • Wide cavity. • Natural convection. • Buoyancy-driven. • Only experiment. • Experiment was performed with water as the fluid.	• Modelled in 2D.	• Two different cases: – Asymmetrically heated vertical channel with one side 10°C warmer than the fluid and the other side 10°C colder than the fluid. – Symmetrically heated vertical channel with both sides 20°C warmer than the fluid.			• Performed experiment. • References: (A) Boudjemadi et al. (1997), (B) Fedorov and Viskanta (1997), (C) Versteegh and Nieuwstadt (1998).	• For the symmetrically heated channel, a zone with potentially reverse flow appeared at the top's centerline. • For the asymmetrically heated channel, there appear two opposite boundary layers that create an internal vortex if one side is colder than the ambient fluid.	• The flow is considered turbulent for values of Rayleigh numbers ≥105 (reference (A), (B) and (C)).	• $Aspr$=3.125 • Ra_D=10^5
Polidori et al. 2015	• Unsteady state. • Wide cavity. • Natural convection. • Buoyancy- driven. • Only experiment. • Experiment was performed with water as the fluid. • Re-circulation.	• Modelled in 2D.	• An asymmetrically heated channel: – One wall with no heat flux. – One wall with a heat flux in the middle and no heat flux in the top and bottom.			• Did experiment. • References: (A) Ospir et al. (2012).	• For asymmetrically heated channel flow, a recirculation cell flow will form, no matter the heat flux.	• The flow patterns are identified according to a modified Rayleigh number. • The experiment is also visualised in reference (A).	• $Aspr$=5.2 • Ra_D=10^5–10^6
Popa et al. 2012	• Laminar flow. • Steady state. • Wide cavity. • Natural convection. • Buoyancy- driven. • Experiment was performed with water as the fluid. • Re-circulation.	• Modelled in 2D. • Channel located in a water tank.	• Local Bernoulli relation at the inlet (pressure inlet). • Zero relative pressure at the outlet. • An asymmetrically heated channel: – One wall with no heat flux. – One wall with a heat flux in the middle and no heat flux in the top and bottom.	• Neglected.	• Not mentioned (most likely irrelevant, as the flow is laminar).	• No experiment. • Validated based on reference (A). • References: (A) Ospir et al. (2012)	• Over-predicted the total recirculation length by 6%. • Not able to model the second recirculation.		• $Aspr$=5– 7 • Ra_D=10^6–10^7
Taieb et al. 2013	• Laminar flow. • Unsteady state. • Wide cavity. • Natural convection. • Buoyancy-driven.	• Modelled in 2D.	• Pressure inlet. • Pressure outlet. • An asymmetrically heated channel: – One wall with no heat flux. – One wall with a heat flux in the middle and no heat flux in the top and bottom.	• Not mentioned.	• Not used (in the laminar regime).	• No experiment. • Validated based on reference (A). • References: (A) Webb and Hill (1989).	• Lower Rayleigh numbers mean the flow is in the developed regime (streamlines parallel to the walls). • Higher Rayleigh numbers cause the flow to become a boundary layer type flow (acceleration near the heated surface and a recirculation zone).	• The flow patterns are identified according to a modified Rayleigh number.	• $Aspr$=5 • Ra_D=10^2–10^5

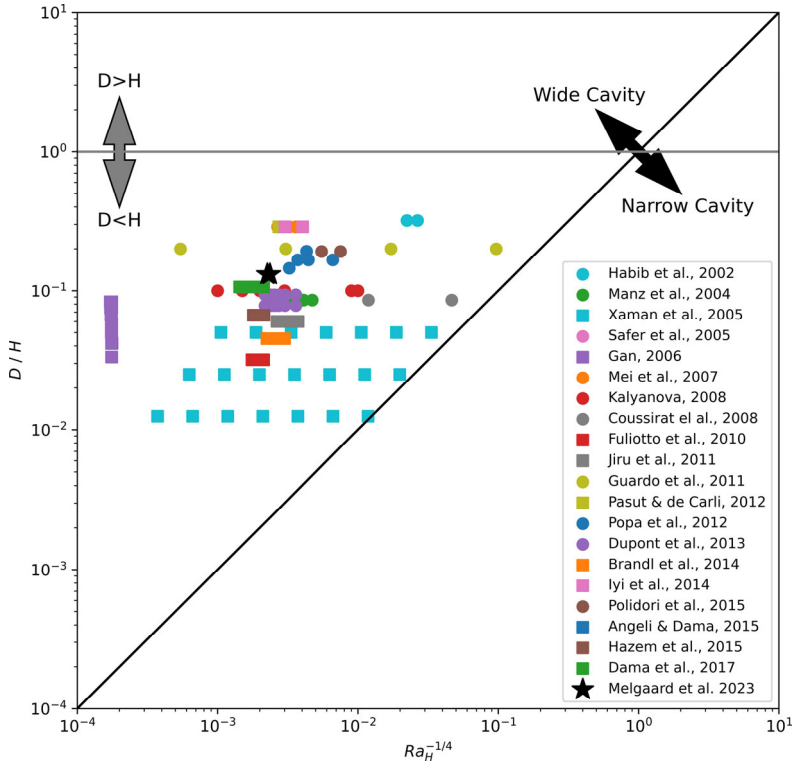

Fig. 7 Distribution of $Ra_H^{-1/4}$ in investigated literature. This data can be visualised in an online interactive table by Melgaard et al. (2023)

suitable TVM for DSF, regardless of the specific scenario being simulated. The issue with this assumption is that DSF flow varies with indoor/outdoor boundary conditions, and considering that one model fits all is not yet proven. Future investigations of DSF modelling could be performed in the same way as in the study by Zhang et al. (2007), where different cases (not only DSFs) have been analysed with a focus on the TVMs' ability to predict the temperature and velocity fields.

2.5.2 *Radiation modelling*

The radiation modelling approach depends on the experiment available at hand. From the research point of view, it is easy to use the constant temperature boundary, as these are simple to identify from existing experimental data and numerical simulations. On the contrary, from an engineering perspective, the CFD model is often developed for performance evaluation where the surface temperatures or surface heat fluxes can be part of the problem to be solved.

2.5.3 *2D and 3D models*

It appears that the studies do not agree on whether 2D or 3D cases present the most accurate results. Even though the flow can be assumed to be bi-directional, studies such as Popa et al. (2012) observed that the numerical 2D model fails to predict recirculation zones. A study by Coussirat et al. (2008) forces the 2D model to act like a 3D by widening the geometry by 10 mm. This method is interesting since the domain may not be large enough to present 3D flow phenomena. Fuliotto et al. (2010) found that the velocity field has strong 3D effects, while the temperature field is in 2D. The study concludes that the model is nearly two-dimensional, meaning that the assumption of bi-directional flow may not be correct, but it might be valid if only the temperature is investigated. The disagreement in dimension modelling between studies suggests a more thorough investigation where the temperature and velocity fields can be compared in 2D and 3D cases.

2.5.4 *External domain modelling*

A lack of consensus is observed on the necessity of modelling the external domain. Iyi et al. (2014) state that "... it is recommended to model the DSF channel in isolation if the outdoor or indoor spaces are not key factors for the airflow and heat transfer. However, the outdoor and the indoor thermal boundary conditions must be well defined." Pasut and de Carli (2012) state that: "...the external environment modelisation is important for the simulation quality. An adequate ambient air frees the user from deciding the air inlet direction and makes this more reliable." These two statements do not seem to agree on the method despite being based on the same experimental data from Mei et al. (2007). However, it should be noted that these studies are made with natural ventilation.

2.5.5 *Modelling glass boundaries*

From the current review study, no consensus appears on which radiation model should be used for different DSF configurations. It is thus not possible to conclude whether the radiation model should be directly implemented or accounted for by constant temperature or constant flux boundaries.

3 Case study

To address the lack of validation procedures for DSF systems, a detailed case study is presented. It focuses on two key aspects. Firstly, it investigates the importance of velocity, temperature, or both in validating a model using empirical data. Secondly, it examines and compares different TVM and radiation models to determine their performance in this particular case.

While assessing modelling strategies for the surrounding domains (as in Figure 3) is relevant, it was not possible within the scope of this study due to the constraints imposed by the experimental setup. Specifically, the outdoor environment in the setup lacks a radiation source, and the indoor environment is represented by a heated surface (see Section 3.1). As a result, the developed CFD models are solely focused on the strategy defined in Figure 3(d).

3.1 Experimental method and setup

The experimental results, which were used as a basis for evaluating the performance of the different CFD models regarding the fan-assisted convection flow of the DSF, came from the baseline case of Todorova and Dimitrov (2016). The experimental setup was installed in the indoor environment and energy engineering laboratories of Aalborg University (Denmark). The setup contained a mechanically-controlled inlet that could adjust the temperature and velocity of the supply air. A heat mat was installed on the back wall to control the boundary condition, thereby removing the influence of an indoor environment. The power of the heat mat was regulated using a PID controller, with a measuring interval of 2 seconds. Velocity measurements were conducted using the laser-Doppler method (Dantec LDA). The configuration of the LDA system used in the measurement is shown in Table 3.

For each air velocity point measurement, 15,000 samples are collected to ensure a data validation rate of 99% and a Gaussian sample distribution to minimize errors in the data sampling. The uncertainty for this type of measurement is estimated to be below 0.0038 m/s (Yeh and Hall 2008; Esteifi 2011; Shinder et al. 2015). The temperature was measured using calibrated thermocouples type K with a measurement uncertainty of 0.09 K (2σ confidence interval). The placement of the measurement points can be seen in Figure 8.

The layout of the test DSF and the parameters used as boundary conditions can be seen in Figure 9 and Table 4, respectively. The experiment was carried out under steady-state conditions.

Besides the boundary conditions used for the experiment, the air properties associated with the experiment can be found in Table 5.

Based on the results from the baseline case, six dimensionless numbers were calculated using the middle of the cavity as the reference point (see Table 6). This choice is essential, as the dimensionless numbers will vary depending on where the reference is taken. The reference values can be seen in Table 7. The complete list of dimensionless numbers

Table 3 LDA configuration

Laser type	Helium-Neon laser
Wavelength	623.8 nm (red)
Focal length	400 mm
Beam diameter	1.35 mm
Expander ratio	1
Beam spacing	38 mm

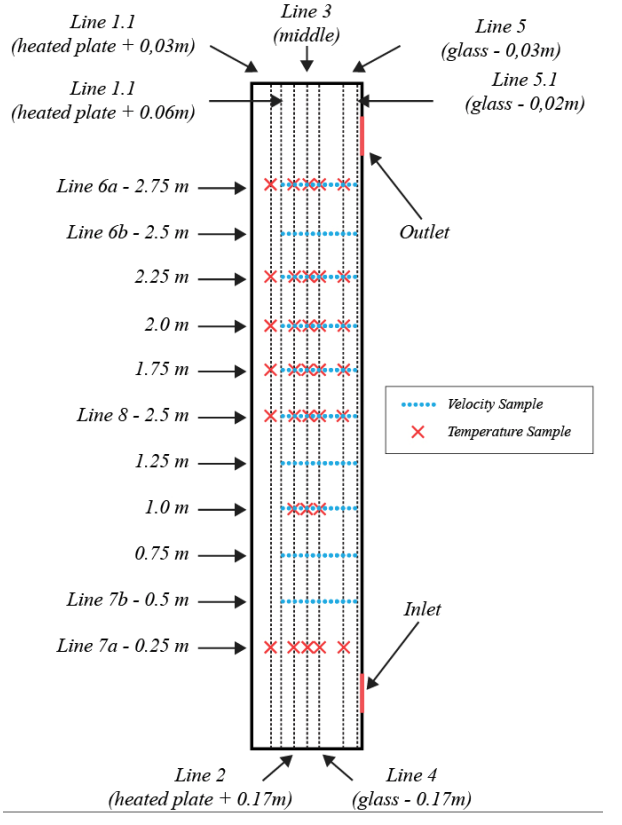

Fig. 8 Velocity and temperature measurement points adapted from Todorova and Dimitrov (2016)

Table 4 Boundary conditions for the baseline case of Todorova and Dimitrov (2016) and CFD simulation

Geometry	Type	CFD boundary condition	Velocity	Thermal
Inlet	Mechanically controlled inlet	Velocity inlet	0.021 m/s	15.77 °C
Outlet	Outlet	Pressure outlet	—	23.72 °C
Front wall	Wall	No slip	—	26.02 °C
Heated back wall	Wall	No slip	—	27.91 °C
Miscellaneous geometry	Wall	No slip	—	0 W/(m^2·K)

Table 5 Air properties for the baseline case

Parameter	Value
Density (ρ)	1.204 kg/m^3
Specific heat capacity (C_p)	1007 J/(kg·K)
Thermal conductivity (k)	0.02514 W/(m·K)
Kinematic viscosity (ν)	$1.47{\cdot}10^{-5}$ m^2/s
Expansion coefficient (β)	$3.5{\cdot}10^{-3}$ K^{-1}

Table 6 Dimensionless numbers for the baseline case

Parameter	Surface temperature on the front wall ($T_{surf\_front\_wall}$)	Surface temperature on the heated back wall ($T_{surf\_heated\_backwall}$)
Aspect ratio (Aspr)	7.625	7.625
Prandtl (Pr)	0.7082	0.7082
Grashof (Gr_D)	$1.03{\cdot}10^8$	$1.22{\cdot}10^8$
Reynolds (Re_D)	$0.87{\cdot}10^2$	$0.87{\cdot}10^2$
Archimedes (Ar_D)	$1.35{\cdot}10^4$	$1.60{\cdot}10^4$
Rayleigh (Ra_D)	$7.31{\cdot}10^7$	$8.66{\cdot}10^7$

Table 7 Reference values for calculation of dimensionless values

Parameter	Value
Characteristic length (L_D)	0.40 m
Height (H)	3.05 m
Depth (D)	0.40 m
Ambient temperature (T_{amb})	15.77 °C
Surface temperature on the front wall ($T_{surf\_front\_wall}$)	26.02 °C
Surface temperature on the heated back wall ($T_{surf\_heated\_backwall}$)	27.91 °C
Average velocity at horizontal cross-section (u_{avg})	0.0032 m/s

from this case can be visualised in an online interactive table (Melgaard et al. 2023) along with those from the investigated literature. These dimensionless numbers are needed to compare any new investigations to the ones already found in the literature. Indeed, simply comparing, e.g., the inlet temperature of the different cases, does not tell much about the expected behaviour of the DSF because this would also depend on the ratio between buoyant and gravitational forces.

3.2 CFD models and description

Based on the empirical results from the experimental setup described above, a CFD model was created in both a 2D and 3D version. The geometry and main boundary conditions are described in Figure 9. The inlet was modelled as a velocity inlet with a turbulence intensity of 9%. The outlet was modelled as a pressure outlet with a turbulence intensity of 9%. It thus ensures the possibility of backflow, where a part of the outlet expels the air while another part takes some of the air into the cavity. The heated back wall and the front wall were both maintained at constant temperatures. The rest of the cavity's surfaces had a zero heat flux condition: they were well insulated, and the temperature difference between the DSF and the surrounding laboratory air was very small. For the 2D case, the model represents a cut through the centre of the DSF, with the boundary conditions being analogous to the 3D case.

With the purpose of testing which TVMs and radiation models are most suited for simulating a DSF, nine different TVMs were chosen, ranging from the simple SA model to the advanced Reynolds stress LPS model. Of these nine models, the three k-ε models were tested for both scalable and enhanced wall functions. Furthermore, three different radiation models were simulated to compare with cases without a radiation model. All the different combinations of TVMs and radiation models in 2D simulations can be found in Table 12. The simulated 3D cases are chosen based on the results from the 2D simulations and can be found in Table 14.

The CFD simulations were conducted using ANSYS 18.0 software. The meshes were generated with the ICEM CFD software. Mesh independence tests were performed as shown in Table 10. For example, the 39k mesh has a minimum orthogonality of 1.00, a maximum aspect ratio of 1.47 and was completely uniform. It was a deliberate decision to ensure a well-resolved, uniform mesh in all areas of the DSF, given the limited understanding of the flow structure and the presence of local phenomena. Further discussion on this can be found in Section 3.4. The parameters used for all the CFD models are summarized in Table 8. The majority of the presented results in this study are derived from models that have achieved convergence. For the few cases in which no convergence was reached, the presented results are labelled as "Not converged".

3.2.1 *Criteria for determining mesh independence*

Evaluating the mesh independence of the various meshes was done using the velocity and temperature at different lines throughout the DSF. For the 2D case, three vertical lines (3 cm from both the front and back wall, as well as in the middle) and five horizontal lines (25 and 50 cm from

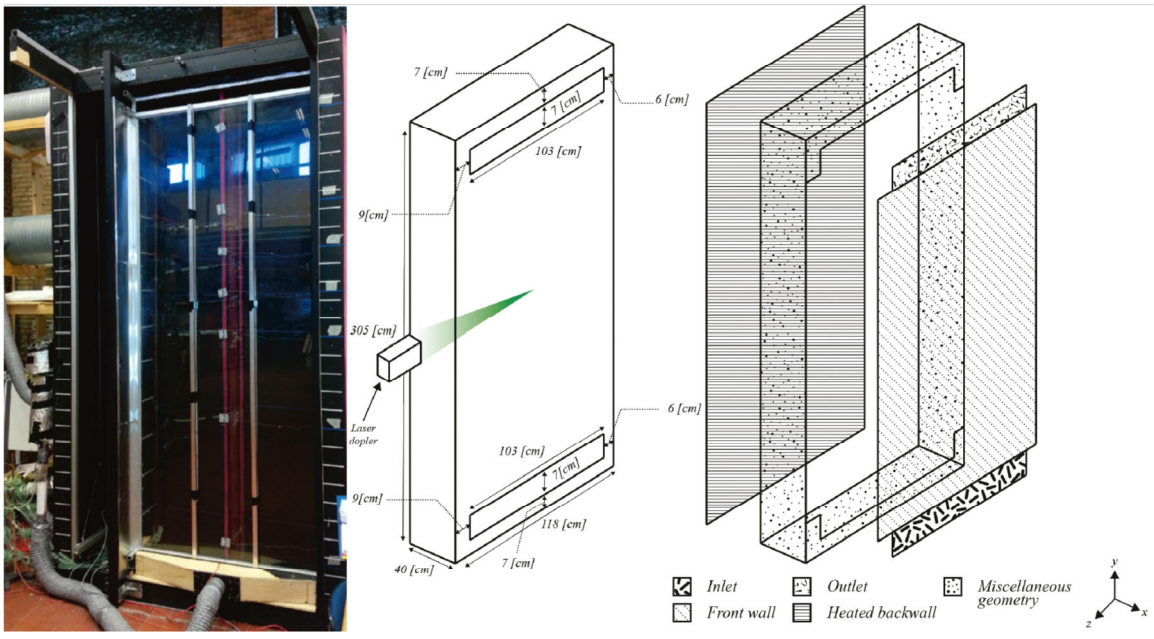

Fig. 9 Geometry of the 3D CFD simulation case and the position of the different boundaries

Table 8 CFD parameters used for all the models

Solver		**Pressure-Velocity coupling**	
Solver type	Pressure-based	Scheme	SIMPLE
Velocity formulation	Absolute		
Time condition	Steady state		
Convergence criteria		**Spatial discretization**	
Continuity	10^{-9}	Gradient	Least squares cell-based
x-velocity	10^{-9}	Pressure	Second order
y-velocity	10^{-9}	Momentum	Second order upwind
Energy	10^{-13}	Turbulent kinetic energy	First order upwind
k	10^{-9}	Turbulent dissipation rate	First order upwind
Epsilon	10^{-9}	Energy	Second order upwind
Massflow rate between inlet and outlet	10^{-6}		

both the top and bottom, as well as in the middle) were used to capture the behaviour in the different zones of the DSF. The entire dynamics of the DSF can thus be assessed, as opposed to just taking a few points. This ensures that no areas are modelled inadequately.

For the 3D case, there were five vertical lines (one in the middle of the DSF, one 3 cm into the cavity from the centre of the front wall, the same for the back wall, one 19 cm into the cavity from the centre of each sidewall) and three horizontal lines (all of them going from sidewall to sidewall and having 20 cm to both the front and back wall, they are 50 cm, 150 cm and 250 cm from the bottom of the cavity).

The criteria for determining mesh independence were set as <10% deviation between the average velocities, <10% deviation between the maximum velocities, <1% deviation between the average temperature in °C, and <1% deviation between the maximum temperatures measured in °C. Table 9 shows that as the models become more complex, the need for a higher mesh resolution increases. The green markings in the table indicate the independent meshes used for further simulation of 2D cases. One can find the results of the mesh independence tests in Table 9.

For the k-ε RNG CFD model without radiation and with the scalable wall function, when tested for mesh independence, one can observe that the 39k mesh is the first mesh-independent configuration (using the 160k mesh as the reference and the criteria mentioned earlier). All the criteria are evaluated for each mesh independence test, as shown in Table 10. An example of the mesh, along with

velocity and temperature profiles in the DSF for the 39k mesh with scalable wall function and no radiation model, can be seen in Figure 10.

3.3 Results and comparison

The grading system used in this article is an expanded version of the one from Pasut and de Carli (2012) where the A+ and C+ grades have been added: the A ratings are good results, the B ratings are acceptable results, the C ratings are marginally acceptable results, and the D ratings are poor results. The deviation for the temperature is calculated based on the difference between the measured and calculated temperature divided by the measured temperature in °C, meaning that rating A will generally be for deviations lower than 1.4–2.7 °C depending on location in the DSF. The same methodology applies to the velocity, where the deviation is calculated as the difference between

Table 9 Meshes tested for independence of the 2D case are marked in yellow, while green marks the independent meshes

TVM	Radiation model	Wall function	8k	18k	39k	80k	160k	320k	640k
k-ε RNG	No	Scalable							
	Yes	Scalable							
	No	Enhanced							
	Yes	Enhanced							
k-ω SST	Yes	—							
Transition SST	Yes	—							
Reynolds Stress LPS	Yes	Enhanced							

Table 10 Example of mesh independence test for *k*-ε RNG with scalable wall function and no radiation model (all the lines can be found directly in Figure 8)

Criteria	Line	Limit (using the 160k mesh as reference)	8k mesh	18k mesh	39k mesh	80k mesh
Average temperature deviation	1	0.2293	0.1174	0.1357	0.0791	0.0285
	3	0.2291	0.1032	0.1266	0.0769	0.0302
	5	0.2282	0.1069	0.1203	0.0715	0.0260
	6a	0.2529	0.0243	0.0557	0.0413	0.0249
	7a	0.1874	0.1491	0.0561	0.0257	0.0143
	8	0.2436	0.2121	0.2127	0.1165	0.0385
Maximum temperature deviation	1	0.2588	0.2737	0.2643	0.1479	0.0494
	3	0.2556	0.2880	0.2776	0.1624	0.0532
	5	0.2549	0.2592	0.2626	0.1487	0.0501
	6a	0.2791	0.0656	0.0784	0.0525	0.0330
	7a	0.2791	0.1810	0.0691	0.0315	0.0169
	8	0.2791	0.2614	0.2460	0.1317	0.0428
Average velocity magnitude deviation	1	0.0036	0.0039	0.0027	0.0013	0.0005
	3	0.0008	0.0006	0.0013	0.0008	0.0004
	5	0.0026	0.0041	0.0030	0.0017	0.0007
Maximum velocity magnitude deviation	1	0.0088	0.0166	0.0130	0.0072	0.0028
	3	0.0070	0.0046	0.0118	0.0070	0.0032
	5	0.0118	0.0285	0.0178	0.0107	0.0052
Average vertical velocity deviation	6b	0.0044	0.0026	0.0019	0.0011	0.0005
	7b	0.0003	0.0001	0.0002	0.0001	0.0000
	8	0.0003	0.0004	0.0001	0.0000	0.0000
Maximum vertical velocity deviation	6b	0.0105	0.0077	0.0058	0.0034	0.0016
	7b	0.0029	0.0009	0.0007	0.0005	0.0002
	8	0.0034	0.0018	0.0006	0.0001	0.0001

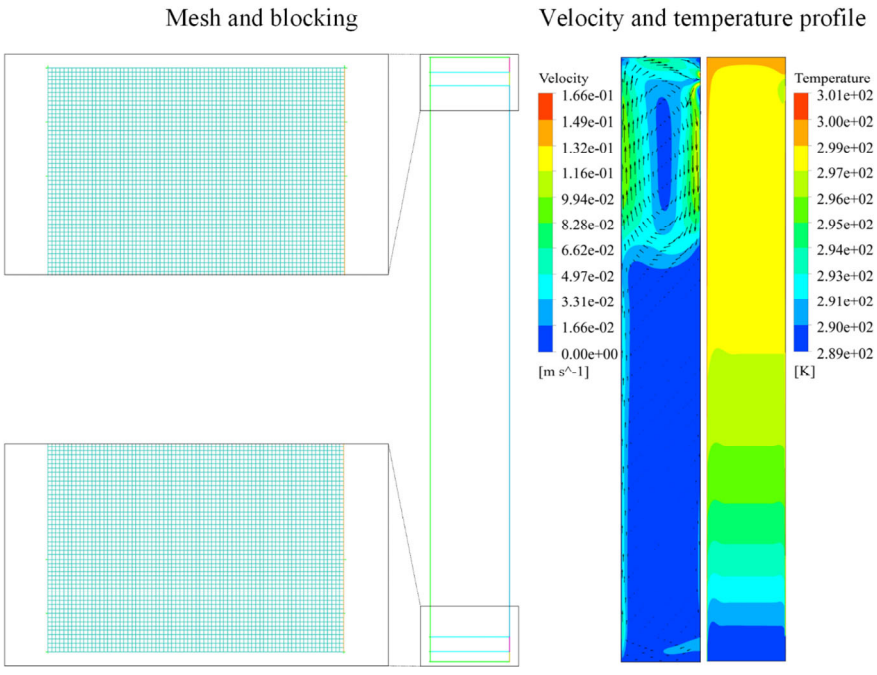

Fig. 10 Example of mesh and blocking for the 39k mesh, along with the velocity and temperature profiles for the case with scalable wall function and no radiation model

the measured and modelled velocity divided by the measured velocity, meaning that rating A will generally be for deviations lower than between 0.002 and 0.012 m/s depending on location in the DSF.

Figure 8 shows the data extraction lines for temperature and velocity for the CFD simulations based on the measurement conducted by Todorova and Dimitrov (2016) (used as the baseline). All the different combinations of TVMs and radiation models are checked against the measured results from the baseline case, using the grades from Table 11. The results are presented in Table 12 and Table 13.

3.3.1 2D Model

One can observe from the simulation results that the *k*-ε models generally perform better than others. This is especially the case when considering computation intensity: the mesh for the Reynolds stress LPS model, which performed similarly to the *k*-ε models, requires twice as many control volumes. The *k*-ε models can account for buoyancy-driven flow, but the enhanced wall function is needed to get acceptable results. This wall function should always be used when modelling buoyancy-driven flow in a DSF, as the general deviation is reduced by 20%–30%.

Regarding the radiation models, "no model" and S2S appear to perform slightly better than the others in terms of velocity accuracy, but the DO is slightly better for the temperature field. In general, the difference between radiation models is small. Therefore, it is difficult to conclude which is performing best as it is most likely case-dependent. One can see from Table 13 that the temperature modelling with a deviation below 5% is not a problem for most of the models, albeit the temperature at the inlet height (0.25 m) is generally within a deviation of 10%. This indicates that accuracy on the temperature profile predictions might not be a good key performance indicator to validate models, as most models will perform well in that regard. However, they might perform poorly for the velocity field prediction, as seen in the SA–S2S test: the models have an A+ grade for almost all temperature predictions, while the velocity prediction accuracy is generally around C+ (see Table 12 and Table 13).

Depending on whether the priority for the model's accuracy is on the velocity field prediction or the temperature field prediction, optimal parameter choices will differ. One can see from Table 12 that the best combination of TVM, wall function and radiation model for predicting the velocity

Table 11 Grades used to evaluate the difference between the CFD and measured results

Grade	Deviation
A+	< 5%
A	< 10%
B+	< 20%
B	< 30%
C+	< 40%
C	< 50%
D	> 50%

Table 12 Grades for the different TVMs, wall functions (for *k*-ε) and radiation models for air velocity in 2D

TVM	Radiation model	Height from the bottom of the DSF in meters										Total
		0.50	0.75	1.00	1.25	1.50	1.75	2.00	2.25	2.50	2.75	
SA	—	C	B	B+	B	C+	A	B	C+	D	C	C+
	S2S	C	B	B+	C+	C+	A	B	C+	D	C	C+
k-ε standard (scalable)	—	C	D	C	C+	C+	D	C	C	D	D	C
	S2S	C+	C	C	B	B	D	C+	C+	C	D	C+
k-ε standard (enhanced)	—	B+	A+	A	A	B+	C+	B+	B+	A+	A+	B+
	S2S	B+	A+	A+	A	B+	B	B+	B+	A+	A+	B+
k-ε RNG (scalable)	—	C+	C	C+	B	B+	C	C+	C+	C	D	C+
	S2S	B	C+	C+	B+	A	C+	B	B	C+	C	B
k-ε RNG (enhanced)	—	B	A	A+	B+	B	B	B+	B	A+	A+	B+
	S2S	B	A	A+	B+	B	B	B+	B	A+	A+	B+
	DO	B	A	A	B	B	B	B	B	A	A	B+
	P-1	B	A	A	B	B	B	B+	B	A	A+	B+
k-ε realisable (scalable)	—	C+	C+	C+	B	B+	C	C+	C+	C+	C	C+
	S2S	B	B	B	B+	A	C+	B	C+	C+	C	B
k-ε realisable (enhanced)	—	B+	A+	A+	B+	B+	B	A	A	A	A+	B+
	S2S	B	A+	A+	B+	B	B	A	A	A	A+	B+
	DO	B	A	A+	B+	B	B	A	B+	A+	A+	B+
	P-1	B	A	A+	B+	B	B	A	B+	A+	A+	B+
k-ω standard	—	B	B+	A	B	B	B	B	C+	B+	B+	B
	S2S	B	B+	B+	B	B	B	B	C+	B+	B+	B
k-ω SST	—	B	A	A+	C+	D	C+	D	D	D	D	D
	S2S	B	A	A	C+	D	C+	D	D	D	D	D
Transition SST	—	A+	B	B+	A	C+	A+	C	D	D	B	C+
	S2S	A+	B+	B+	A+	B	A+	C	D	D	B	B
Transition *k-kl- ω*	—	Not converged										
	S2S	Not converged										
Reynolds stress LPS	—	Not converged										
	S2S	A+	B+	B+	A+	A	B	A+	B+	C	B+	B+

field is the *k*-ε Realisable with the enhanced wall function and no radiation model. On the other hand, Table 13 indicates that the best combination for modelling the temperature field is either the SA with S2S or the *k*-ε RNG/*k*-ε Realisable with enhanced wall treatment and the DO radiation model.

In these cases, model combinations optimising the accuracy of the velocity field predictions will also produce good predictions of the temperature field. On the contrary, model combinations optimising the accuracy of the temperature field predictions yield poor predictions of the velocity field in a third of the cases.

3.3.2 3D Model

Based on the results from the 2D case, it was chosen to test the *k*-ε RNG model with enhanced wall treatment in 3D with the different radiation models available. The mesh independence was achieved at 3.4 million nodes, using the same evaluation criteria as in the 2D mesh independence test. As shown in Table 14, the radiation models either performed poorly for the velocity predictions or did not converge. The only CFD model performing acceptably in most of the areas of the DSF was the one without a radiation model, which just used a constant temperature on the wall boundaries, although it struggled in the area around the outlet. This was most likely due to the potential non-stationary flow that can occur around an outlet of this type, where backflow is possible.

As shown in Table 15, the temperature predictions for all the models were generally within the A+ rating, similar to the 2D case. This is because the temperature is relatively easy to predict compared to velocity.

Table 13 Grades for the different TVMs, wall functions (for *k*-ε) and radiation models for temperature in 2D

TVM	Radiation model	Height from the bottom of the DSF in meters							Total
		0.25	1.00	1.50	1.75	2.00	2.25	2.75	
SA	—	A	A+	A+	A+	A+	A+	A+	A+
	S2S	A+	A+	A+	A+	A+	A+	A+	A+
k-ε standard (scalable)	—	B	B+	B+	A	A	A	A	B+
	S2S	B+	B+	A	A	A	A	A	A
k-ε standard (enhanced)	—	A	A+	A+	A+	A+	A+	A+	A+
	S2S	A	A+	A+	A+	A+	A+	A+	A+
k-ε RNG (scalable)	—	B	B+	A	A	A	A	A	B+
	S2S	B+	A	A	A	A	A	A	A
k-ε RNG (enhanced)	—	A	A+	A+	A+	A+	A+	A+	A+
	S2S	A	A+	A+	A+	A+	A+	A+	A+
	DO	A+	A+	A+	A+	A+	A+	A+	A+
	P-1	A	A+	A+	A+	A+	A+	A+	A+
k-ε realisable (scalable)	—	B	B+	A	A	A	A	A	B+
	S2S	B+	A	A	A	A	A	A	A
k-ε realisable (enhanced)	—	A	A+	A+	A+	A+	A+	A+	A+
	S2S	A	A+	A+	A+	A+	A+	A+	A+
	DO	A+	A+	A+	A+	A+	A+	A+	A+
	P-1	A	A+	A+	A+	A+	A+	A+	A+
k-ω standard	—	A	A+	A+	A+	A+	A+	A+	A+
	S2S	A	A+	A+	A+	A+	A+	A+	A+
k-ω SST	—	A	A+	A+	A+	A+	A+	A+	A+
	S2S	A	A+	A+	A+	A+	A+	A+	A+
Transition SST	—	B+	A+	A+	A+	A+	A+	A+	A+
	S2S	A	A+	A+	A+	A+	A+	A+	A+
Transition *k-kl- ω*	—	Not converged							
	S2S	Not converged							
Reynolds stress LPS	—	Not converged							
	S2S	A	A+	A+	A+	A+	A+	A+	A+

Table 14 Grades for the different radiation models for air velocity in 3D

TVM	Radiation model	Height from the bottom of the DSF in meters										Total
		0.50	0.75	1.00	1.25	1.50	1.75	2.00	2.25	2.50	2.75	
k-ε RNG (enhanced wall function)	—	B+	A+	A+	B+	B+	B	A+	B+	D	C	B+
	DO	A+	B	C+	C	C+	C	D	D	D	D	D
	P-1	B	C	D	C	A	A+	D	D	D	D	D
	S2S	A+	B	C+	C	C+	C+	D	D	D	D	D
	Rosseland	Not converged										
	MC	Not converged										

Table 15 Grades for the different radiation models for temperature in 3D

TVM	Radiation model	Height from the bottom of the DSF in meters							Total
		0.25	1.00	1.50	1.75	2.00	2.25	2.75	
k-ε RNG (enhanced wall function)	—	A	A+	A+	A+	A+	A+	A+	A+
	DO	A+	A+	A+	A+	A+	A+	A+	A+
	P-1	A+	A+	A+	A+	A+	A+	A+	A+
	S2S	A+	A+	A+	A+	A+	A+	A+	A+
	Rosseland	Not converged							
	MC	Not converged							

3.4 Discussion

The current literature review indicates that many of the previous investigations are based on models validated only for the temperature field (temperature measurements). On the one hand, this approach is reasonable if the temperature field is the study's primary objective. Nevertheless, if the model is meant to predict the velocity field or evaluate naturally induced airflow rates, relying solely on temperature field validation may be inadequate.

The presented case study, where CFD simulations were compared against empirical data, has demonstrated that the ability of a model to accurately predict the temperature field does not necessarily imply an accurate prediction of the velocity field. Neglecting the prediction of the velocity field can have critical consequences when evaluating DSF performance under different boundary conditions. Hence, the authors advocate for velocity measurements alongside temperature measurements in the validation of DSF CFD models. Both temperature and velocity fields should be given equal significance and predicted with acceptable accuracy by the considered CFD model.

In addition to relying solely on temperature for validation, some models are also validated using only a few points, such as inlet and outlet temperature or velocity. While this approach confirms potential validity, it does not ensure the accuracy of the velocity and temperature fields. Therefore, it is crucial to measure at least some points inside the DSF for validation, ensuring that the key flow elements are adequately captured. However, this presents a challenge as acquiring highly detailed experimental data may not be feasible due to limitations in existing measurement techniques (Giancola et al. 2018).

A relevant aspect of CFD model validation and comparison is the metric and grading schema employed for benchmarking. In the present study, the deviation between the measured and simulated temperature and velocity values are normalized by the measured values and then categorized into a grading system (A+, A, B, etc). While this approach has been utilized in several publications, it has limitations in terms of the physical interpretation of the results. Future studies could aim to develop alternative metrics and grading schemas with stronger physical interpretations to obtain a more nuanced evaluation of the models' performance.

A paper by Gau et al. (1992) suggests that the flow inside a vertical heated channel has transient behavior for $Ar > 48$. It is important to note that comparing transient measurements to steady-state CFD models can pose challenges, as the mean value of the flow may not adequately represent its time-dependent characteristics. Although the potential for transient flow has not been addressed in this study, it is essential to acknowledge its possibility. Similarly, the existence of flow reversal or recirculation zones in the cavity is another aspect of the flow structure that must be recognized.

In Figure 10, the temperature and velocity profiles display the simultaneous ingress and egress of air through the top opening of the DSF, as depicted in the CFD model. The presence of this phenomenon is not only crucial for constructing an accurate CFD model but also necessary for model validation and comparison with other models. For instance, in the presence of flow reversal, metrics commonly used for DSF evaluation, such as the mass-flow rate or the heat removed from the cavity, need to be calculated with greater care. In this study, due to the unavailability of empirical data on the in- and out-flow through the top opening, these metrics were omitted from the evaluation.

To capture potential local phenomena (i.e., reversal or recirculation zones) in the flow structure, a well-resolved uniform mesh was used in all models of this study. In Figure 10, these phenomena evidently appear in the upper part of the cavity. However, a systematic study of these phenomena has not been conducted (as discussed in Section 2.1.2), and with the current state of the art for DSF, it is not possible to identify them beforehand for optimal mesh generation with finer resolution in the regions of local phenomena. In this context, Figure 7 allows for the identification of existing studies with potentially similar physical behavior and flow structure. As more studies are added to the Figure 7 database, it will become easier for modellers to assess the local phenomena in comparable studies and to thus draw stronger conclusions.

To enhance the comparability of flow types and flow structures in different CFD studies on DSF (and thus facilitate the selection of suitable turbulence models), the authors of this review recommend systematic reporting of key dimensionless numbers in scientific publications. These numbers include the cavity aspect ratio, Rayleigh number, Reynolds number, and Prandtl number. To ensure clarity, it is essential to specify the characteristic length of the cavity and the location used for the calculation of these dimensionless numbers, as they can vary significantly depending on the assessment point's location within the DSF cavity.

4 Conclusions

This study investigated the simulation trends of DSF with CFD and the influences that different CFD configurations and settings have on the simulation accuracy. A series of 2D and 3D CFD simulations, with variations in TVMs, wall treatments, and radiation modeling, are compared against measurements of velocity and temperature in a DSF to determine the most appropriate CFD settings.

The accuracy of both 2D and 3D models is comparable; however, the 3D model seems to be more affected by the choice of radiation model. This suggests that if strong 3D effects in the cavity are not expected, the 2D model might be sufficient. The study also showed that the accuracy of the simulation results depends on the choice of the TVM model and wall treatment, with the k-ε type and enhanced wall function having the best performance in the case study. The final consideration is whether to use a specific radiation model or model the boundaries with heat flux or temperature. In the 2D case, the S2S model gave the best results, although with a slight difference compared to the other radiation models. In the 3D case, using temperature gradient boundaries and no radiation model clearly produced the best results.

When determining the best-performing model, the ability to predict the velocity field appears to be more critical than the ability to predict the temperature field. This is because a model that predicts the velocity field accurately also predicts the temperature field correctly, but the reverse is not necessarily true.

When the dimensionless numbers are calculated, the value for the velocity changes depending on where the reference point is placed in the DSF. To ensure consistency in terms of the reference velocity used for the calculation of dimensionless numbers, it is suggested to adopt the method applied in the published studies for channel flow. It involves using the average inlet velocity (i.e., the velocity at the bottom cross-section of the channel) as the dimensioning parameter. However, for DSF geometries where the inlet opening size differs from the cross-section, the average velocity in the cross-section of the cavity must be used.

The challenge of DSF measurement and simulation is potentially not a standalone problem, as multiple combinations of boundary conditions and geometries can represent several different heat transfer problems. The attempt to illustrate the spectrum of potentially different performances of DSF is given in Figure 7. This study addresses only one of many scenarios by suggesting CFD settings applicable to this particular problem. Therefore, the authors argue for the active use of a set of key dimensionless numbers (Table 1) to organize the knowledge about DSF within the scientific community, compare case studies, identify relevant experimental data for validation and, when possible, identify suitable CFD settings, for specific DSF configurations.

5 Suggestions for future work

For future work, a broader spectrum of the DSF configurations will be studied experimentally and numerically. Additionally, a PIV measurement technique will be adopted, which captures a velocity field as opposed to the point-based laser Doppler technique used in the experiment by Todorova and Dimitrov (2016).

Funding note: Open access funding provided by Royal Danish Library.

Declaration of competing interest

The authors have no competing interests to declare that are relevant to the content of this article.

Author contribution statement

Simon Pommerencke Melgaard: conceptualisation, methodology, software, validation, formal analysis, investigation, data curation, writing—original draft, writing—review & editing, visualisation, project administration. Ivan Titov Nikolaisson: conceptualisation, methodology, software, formal analysis, investigation, writing—original draft, writing—review & editing, visualisation, project administration. Chen Zhang: conceptualisation, methodology, resources, writing—review & editing, supervision. Hicham Johra: software, resources, data curation, writing—review & editing, visualisation, supervision. Olena Kalyanova Larsen: conceptualisation, methodology, resources, writing—review & editing, supervision, project administration.

References

Ahmadi J, Mahdavinejad M, Larsen OK, et al. (2022). Evaluating the different boundary conditions to simulate airflow and heat transfer in Double-Skin Facade. *Building Simulation*, 15: 799–815.

Allaby M (2008). A Dictionary of Earth Sciences, 3rd edn. Oxford, UK: Oxford University Press.

Amadio C, Bedon C (2012). Elastoplastic dissipative devices for the mitigation of blast resisting cable-supported glazing façades. *Engineering Structures*, 39: 103–115.

Angeli D, Dama A (2015). Modelling natural ventilation in double skin facade. *Energy Procedia*, 78: 1537–1542.

Balocco C (2002). A simple model to study ventilated facades energy performance. *Energy and Buildings*, 34: 469–475.

Bangalee MZI, Miau JJ, Lin SY (2013). Computational techniques and a numerical study of a buoyancy-driven ventilation system. *International Journal of Heat and Mass Transfer*, 65: 572–583.

Barbosa S, Ip K (2014). Perspectives of double skin façades for naturally ventilated buildings: A review. *Renewable and Sustainable Energy Reviews*, 40: 1019–1029.

Bejan A (2013). Convection Heat Transfer, 4th edn. Hoboken, NJ, USA: John Wiley & Sons.

Ben-Mansour R, Habib MA, Badr HM, et al. (2007). Comparison of different turbulence models and flow boundary conditions in predicting turbulent natural convection in a vertical channel with isoflux plates. *Arabian Journal for Science and Engineering*, 32: 191–218.

Bhamjee M, Nurick A, Madyira DM (2013). An experimentally validated mathematical and CFD model of a supply air window: Forced and natural flow. *Energy and Buildings*, 57: 289–301.

Bird RE, Riordan C (1986). Simple solar spectral model for direct and diffuse irradiance on horizontal and tilted planes at the earth's surface for cloudless atmospheres. *Journal of Climate and Applied Meteorology*, 25: 87–97.

Boudjemadi R, Maupu V, Laurence D, et al. (1997). Budgets of turbulent stresses and fluxes in a vertical slot natural convection flow at Rayleigh Ra = 10^5 and 5.4 10^5. *International Journal of Heat and Fluid Flow*, 18: 70–79.

Brandl D, Mach T, Grobbauer M, et al. (2014). Analysis of ventilation effects and the thermal behaviour of multifunctional façade elements with 3D CFD models. *Energy and Buildings*, 85: 305–320.

Catto Lucchino E, Gelesz A, Skeie K, et al. (2021). Modelling double skin façades (DSFs) in whole-building energy simulation tools: Validation and inter-software comparison of a mechanically ventilated single-story DSF. *Building and Environment*, 199: 107906.

Chandrasekhar S (1960). Radiative Transfer. New York: Dover Publications

Chen Q (1995). Comparison of different k-ε models for indoor air flow computations. *Numerical Heat Transfer*, *Part B*: *Fundamentals*, 28: 353–369.

Cherif Y, Sassine E, Lassue S, et al. (2020). Experimental and numerical natural convection in an asymmetrically heated double vertical facade. *International Journal of Thermal Sciences*, 152: 106288.

Chien KY (1982). Predictions of channel and boundary-layer flows with a low-reynolds-number turbulence model. *AIAA Journal*, 20: 33–38.

Choi W, Joe J, Kwak Y, et al. (2012). Operation and control strategies for multi-storey double skin facades during the heating season. *Energy and Buildings*, 49: 454–465.

Choi H, An Y, Kang K, et al. (2019). Cooling energy performance and thermal characteristics of a naturally ventilated slim double-skin window. *Applied Thermal Engineering*, 160: 114113.

Coussirat M, Guardo A, Jou E, et al. (2008). Performance and influence of numerical sub-models on the CFD simulation of free and forced convection in double-glazed ventilated façades. *Energy and Buildings*, 40: 1781–1789.

Dafa'Alla AA, Betts PL (1996). Experimental study of turbulent natural convection in a tall air cavity. *Experimental Heat Transfer*, 9: 165–194.

Dama A, Angeli D, Larsen OK (2017). Naturally ventilated double-skin façade in modeling and experiments. *Energy and Buildings*, 144: 17–29.

Desrayaud G, Chénier E, Joulin A, et al. (2013). Benchmark solutions for natural convection flows in vertical channels submitted to different open boundary conditions. *International Journal of Thermal Sciences*, 72: 18–33.

Ding W, Hasemi Y, Yamada T (2005). Natural ventilation performance of a double-skin façade with a solar chimney. *Energy and Buildings*, 37: 411–418.

Dupont F, Ternat F, Samot S, et al. (2013). Two-dimension experimental study of the reverse flow in a free convection channel with active walls differentially heated. *Experimental Thermal and Fluid Science*, 47: 150–157.

Esteifi K (2011). The Experimental investigation of buoyant flows in inclined differentially heated cavities. PhD Thesis, University of Manchester, UK.

Faggembauu D, Costa M, Soria M, et al. (2003). Numerical analysis of the thermal behaviour of ventilated glazed facades in Mediterranean climates. Part I: development and validation of a numerical model. *Solar Energy*, 75: 217–228.

Favoino F, Goia F, Perino M, et al. (2014). Experimental assessment of the energy performance of an advanced responsive multifunctional façade module. *Energy and Buildings*, 68: 647–659.

Fedorov AG, Viskanta R (1997). Turbulent natural convection heat transfer in an asymmetrically heated, vertical parallel-plate channel. *International Journal of Heat and Mass Transfer*, 40: 3849–3860.

Fluent (2006). FLUENT 6.3 User's Guide. Fluent Inc.

Fuliotto R, Cambuli F, Mandas N, et al. (2010). Experimental and numerical analysis of heat transfer and airflow on an interactive building facade. *Energy and Buildings*, 42: 23–28.

Gan G (2006). Simulation of buoyancy-induced flow in open cavities for natural ventilation. *Energy and Buildings*, 38: 410–420.

Gau C, Yih KA, Aung W (1992). Measurements of heat transfer and flow structure in heated vertical channels. *Journal of Thermophysics and Heat Transfer*, 6: 707–712.

Giancola E, Sánchez MN, Friedrich M, et al. (2018). Possibilities and challenges of different experimental techniques for airflow characterisation in the air cavities of façades. *Journal of Facade Design and Engineering,* 6(3): 34–48.

Gratia E, De Herde A (2007). Are energy consumptions decreased with the addition of a double-skin? *Energy and Buildings*, 39: 605–619.

Guardo A, Coussirat M, Valero C, et al. (2011). CFD assessment of the performance of lateral ventilation in Double Glazed Façades in Mediterranean climates. *Energy and Buildings*, 43: 2539–2547.

Habib MA, Said SA M, Ahmed SA (2002). Velocity characteristics of turbulent natural convection in convergent-plates vertical channels. *International Journal of Fluid Mechanics Research*, 29: 21.

Haddad KH, Elmahdy AH (1998). Comparison of the monthly thermal performance of a conventional window and a supply-air window. *ASHRAE Transactions*, 104(1): 1261–1270.

Hazem A, Ameghchouche M, Bougriou C (2015). A numerical analysis of the air ventilation management and assessment of the behavior of double skin facades. *Energy and Buildings*, 102: 225–236.

He G, Lv D (2022). Distributed heat absorption in a solar chimney to enhance ventilation. *Solar Energy*, 238: 315–326.

Henkes RAWM (1990). Natural-convection boundary layers. PhD Thesis, TU Delft, the Netherlands.

Hottel HC, Sarofim AF (1967). Radiative Transfer. New York: McGraw-Hill.

Inan T, Basaran T (2019). Experimental and numerical investigation of forced convection in a double skin façade by using nodal network approach for Istanbul. *Solar Energy*, 183: 441–452.

Ince NZ, Launder BE (1989). On the computation of buoyancy-driven turbulent flows in rectangular enclosures. *International Journal of Heat and Fluid Flow*, 10: 110–117.

Incropera FP, DeWitt DP, Bergman TL, et al. (2007). Fundamentals of Heat and Mass Transfer, 6th edn. Hoboken, NJ, USA: John Wiley & Sons.

Iyi D, Hasan R, Penlington R, et al. (2014). Double skin façade: Modelling technique and influence of venetian blinds on the airflow and heat transfer. *Applied Thermal Engineering*, 71: 219–229.

Jiru TE, Haghighat F (2008). Modeling ventilated double skin façade—A zonal approach. *Energy and Buildings*, 40: 1567–1576.

Jiru TE, Tao YX, Haghighat F (2011). Airflow and heat transfer in double skin facades. *Energy and Buildings*, 43: 2760–2766.

Jones WP, Launder BE (1972). The prediction of laminarization with a two-equation model of turbulence. *International Journal of Heat and Mass Transfer*, 15: 301–314.

Kalyanova O, Heiselberg PK (2008). Experimental set-up and full-scale measurements in the cube. DCE Technical reports No. 34, Aalborg University, Denmark.

Kalyanova O, Heiselberg P, Felsmann C, et al. (2009). An empirical validation of building simulation software for modelling of double-skin facade (DSF). In: Proceedings of the 11th International IBPSA Building Simulation Conference.

Kim DD (2021). Computational fluid dynamics assessment for the thermal performance of double-skin façades in office buildings under hot climatic condition. *Building Services Engineering Research and Technology*, 42: 45–61.

Li Z (2007). Characteristics of buoyancy driven natural ventilation through horizontal openings. PhD Thesis, Aalborg University, Denmark.

Loonen RCGM, Favoino F, Hensen JLM, et al. (2017). Review of current status, requirements and opportunities for building performance simulation of adaptive facades. *Journal of Building Performance Simulation*, 10: 205–223.

Lops C, Germano N, Matera S, et al. (2021). CFD modelling of naturally ventilated double skin façades: Comparisons among 2D and 3D models. *TECNICA ITALIANA-Italian Journal of Engineering Science*, 65: 330–336.

Manz H, Schaelin A, Simmler H (2004). Airflow patterns and thermal behavior of mechanically ventilated glass double façades. *Building and Environment*, 39: 1023–1033.

Mateus NM, Pinto A, da Graça GC (2014). Validation of EnergyPlus thermal simulation of a double skin naturally and mechanically ventilated test cell. *Energy and Buildings*, 75: 511–522.

Matour S, Garcia-Hansen V, Omrani S, et al. (2021). Wind-driven ventilation of Double Skin Façades with vertical openings: effects of opening configurations. *Building and Environment*, 196: 107804.

Mei L, Infield D, Eicker U, et al. (2003). Thermal modelling of a building with an integrated ventilated PV façade. *Energy and Buildings*, 35: 605–617.

Mei L, Loveday D, Infield D, et al. (2007). The influence of blinds on temperatures and air flows within ventilated double-skin façades. In: Proceedings of Clima 2007, WellBeing Indoors.

Melgaard SP, Nikolaisson IT, Zhang C, et al. (2023). Literature review on Double-Skin Facade systems: Overview of the different scientific studies. Available at https://aau-dsf-overview-web-app.build.aau.dk/. Accessed 22 Feb 2023.

Miyamoto M, Katoh Y, Kurima J, et al. (1986). Turbulent free convection heat transfer from vertical parallel plates. In: Proceeding of the 8th International Heat Transfer Conference.

Modest MF (1993). Radiative Heat Transfer. New York: McGraw-Hill.

Najaf Khosravi SN, Mahdavi A (2021). A CFD-based parametric thermal performance analysis of supply air ventilated windows. *Energies*, 14: 2420.

Nielsen PV, Allard F, Awbi HB, et al. (2007). Computational fluid dynamics in ventilation design REHVA guidebook No_{10}. *International Journal of Ventilation*, 6: 291–294.

Nielsen PV (2015). Fifty years of CFD for room air distribution. *Building and Environment*, 91: 78–90.

Ospir D, Popa C, Chereches C, et al. (2012). Flow visualization of natural convection in a vertical channel with asymmetric heating. *International Communications in Heat and Mass Transfer*, 39: 486–493.

Park CS, Augenbroe G, Sadegh N, et al. (2004). Real-time optimization of a double-skin façade based on lumped modeling and occupant preference. *Building and Environment*, 39: 939–948.

Pastori S, Mereu R, Mazzucchelli ES, et al. (2021). Energy performance evaluation of a ventilated façade system through CFD modeling and comparison with international standards. *Energies*, 14: 193.

Pasut W, De Carli M (2012). Evaluation of various CFD modelling strategies in predicting airflow and temperature in a naturally ventilated double skin façade. *Applied Thermal Engineering*, 37: 267–274.

Polidori G, Fatnassi S, Ben Maad R, et al. (2015). Early-stage dynamics in the onset of free-convective reversal flow in an open-ended channel asymmetrically heated. *International Journal of Thermal Sciences*, 88: 40–46.

Popa C, Ospir D, Fohanno S, et al. (2012). Numerical simulation of dynamical aspects of natural convection flow in a double-skin façade. *Energy and Buildings*, 50: 229–233.

Pourshab N, Tehrani MD, Toghraie D, et al. (2020). Application of double glazed façades with horizontal and vertical louvers to increase natural air flow in office buildings. *Energy*, 200: 117486.

Radhi H, Sharples S, Fikiry F (2013). Will multi-facade systems reduce cooling energy in fully glazed buildings? A scoping study of UAE buildings. *Energy and Buildings*, 56: 179–188.

Saelens D (2002). Energy performance assessment of single storey multiple-skin facades. PhD Thesis, KU Leuven, Belgium.

Saelens D, Roels S, Hens H (2008). Strategies to improve the energy performance of multiple-skin facades. *Building and Environment*, 43: 638–650.

Safer N, Woloszyn M, Roux JJ (2005). Three-dimensional simulation with a CFD tool of the airflow phenomena in single floor double-skin facade equipped with a venetian blind. *Solar Energy*, 79: 193–203.

Safer N (2006). Modélisation des façades de type double-peau équipées de protections solaires: approches multi-échelles. PhD Thesis, INSA Lyon, France.

Sánchez MN, Giancola E, Blanco E, et al. (2019). Experimental validation of a numerical model of a ventilated façade with horizontal and vertical open joints. *Energies*, 13: 146.

Sandberg M, Moshfegh B (1996). Investigation of fluid flow and heat transfer in a vertical channel heated from one side by PV elements, part II - Experimental study. *Renewable Energy*, 8: 254–258.

Seferis P, Strachan P, Dimoudi A, et al. (2011). Investigation of the performance of a ventilated wall. *Energy and Buildings*, 43: 2167–2178.

Shih TH, Liou WW, Shabbir A, et al. (1995). A new *k-ε* eddy viscosity model for high Reynolds number turbulent flows. *Computers and Fluids*, 24: 227–238.

Shinder II, Crowley CJ, James Filla B, et al. (2015). Improvements to NIST'S air speed calibration service. *Flow Measurement and Instrumentation*, 44: 19–26.

Soudian S, Berardi U (2021). Development of a performance-based design framework for multifunctional climate-responsive façades. *Energy and Buildings*, 231: 110589.

Šuklje T, Medved S, Arkar C (2013). An experimental study on a microclimatic layer of a bionic façade inspired by vertical greenery. *Journal of Bionic Engineering*, 10: 177–185.

Taieb S, Ali Hatem L, Balti J (2013). Natural convection in an asymmetrically heated vertical channel with an adiabatic auxiliary plate. *International Journal of Thermal Sciences*, 74: 24–36.

Takemasa Y, Hiraoka M, Katoh M, et al. (2004). Performance of hybrid ventilation system using double-skin facade and vertical airshaft. Kajima Technical Research Institute Annual Report, Kajima Technical Research Institute.

Tao Y, Fang X, Chew MYL, et al. (2021a). Predicting airflow in naturally ventilated double-skin facades: Theoretical analysis and modelling. *Renewable Energy,* 179: 1940–1954.

Tao Y, Zhang H, Huang D, et al. (2021b). Ventilation performance of a naturally ventilated double skin façade with low-e glazing. *Energy*, 229: 120706.

Todorova N, Dimitrov R (2016). Flow nature inside vertical asymmetrically heated channel. Master Thesis, Aalborg University, Denmark. Available at https://projekter.aau.dk/projekter/da/studentthesis/flow-nature-inside-vertical-asymmetrically-heated-channel(118cb29c-f223-432c-8afe-893e56305d0a).html. Accessed 24 Feb 2023.

Versteegh TAM, Nieuwstadt FTM (1998). Turbulent budgets of natural convection in an infinite, differentially heated, vertical channel. *International Journal of Heat and Fluid Flow*, 19: 135–149.

von Grabe J (2002). A prediction tool for the temperature field of double facades. *Energy and Buildings*, 34: 891–899.

Webb BW, Hill DP (1989). High Rayleigh number laminar natural convection in an asymmetrically heated vertical channel. *Journal of Heat Transfer*, 111: 649–656.

Wilcox DC (1988). Multiscale model for turbulent flows. *AIAA Journal*, 26: 1311–1320.

Xamán J, Álvarez G, Lira L, et al. (2005). Numerical study of heat transfer by laminar and turbulent natural convection in tall cavities of façade elements. *Energy and Buildings*, 37: 787–794.

Yeh TT, Hall JM (2008). Uncertainty of NIST Airspeed Calibrations. Gaithersburg, MD, USA: National Institute of Standards and Technology.

Zhang Z, Zhang W, Zhai ZJ, et al. (2007). Evaluation of various turbulence models in predicting airflow and turbulence in enclosed environments by CFD: part 2—Comparison with experimental data from literature. *HVAC&R Research*, 13: 871–886.

Zhang T, Yang H (2019). Flow and heat transfer characteristics of natural convection in vertical air channels of double-skin solar façades. *Applied Energy*, 242: 107–120.